J. Fluid Mech. (2011), *vol.* 683, *pp.* 112–148. © Cambridge University Press 2011
doi:10.1017/jfm.2011.256

Linear and nonlinear stability of floating viscous sheets

G. Pfingstag[1,2,3]†, B. Audoly[2] and A. Boudaoud[3]

[1] Saint-Gobain Recherche, 39 Quai Lucien Lefranc, BP 135, 93303 Aubervilliers CEDEX, France

[2] CNRS and Université Pierre et Marie Curie, Univ Paris 06, UMR 7190, Institut Jean le Rond d'Alembert, Paris, France

[3] Laboratoire de Physique Statistique, École Normale Supérieure, Université Pierre et Marie Curie, Université Paris Diderot, CNRS, 24 rue Lhomond, 75005 Paris, France

(Received 23 August 2010; revised 30 March 2011; accepted 4 June 2011; first published online 19 August 2011)

We study the stability of a thin, Newtonian viscous sheet floating on a bath of denser fluid. We first derive a general set of equations governing the evolution of a nearly flat sheet, accounting for geometrical nonlinearities associated with moderate rotations. We extend two classical models by considering arbitrary external body and surface forces; these two models follow from different scaling assumptions, and are derived in a unified way. The equations capture two modes of deformation, namely viscous bending and stretching, and describe the evolution of thickness, mid-surface and in-plane velocity as functions of two-dimensional coordinates. These general equations are applied to a floating viscous sheet, considering gravity, buoyancy and surface tension. We investigate the stability of the flat configuration when subjected to arbitrary in-plane strain. Two unstable modes can be found in the presence of compression. The first one combines undulations of the centre-surface and modulations of the thickness, with a wavevector perpendicular to the direction of maximum applied compression. The second one is a buckling mode; it is purely undulatory and has a wavevector along the direction of maximum compression. A nonlinear analysis yields the long-time evolution of the undulatory mode.

Key words: nonlinear instability, slender-body theory, thin films

1. Introduction

When a longitudinal compressive force is applied to a thin, elastic rod, the rod remains straight below a well-defined critical force. Above this threshold, the rod bends. This instability, known as buckling, is also relevant to thin viscous threads and sheets. Buckling and, more generally, the dynamics viscous sheets have applications in both natural and industrial processes.

On geological time scales, the earth's crust can be modelled as a stack of superposed thin viscous sheets with different densities and viscosities that float on a denser mantle (Ramberg 1981). Lateral compression of such an assemblage generates phenomena such as folding and mountain-building that can be understood as viscous buckling instabilities (Biot 1964; Johnson & Fletcher 1994; Perazzo & Gratton 2010).

† Email address for correspondence: gilles.pfingstag@gmail.com

https://doi.org/10.1017/jfm.2011.256 Published online by Cambridge University Press

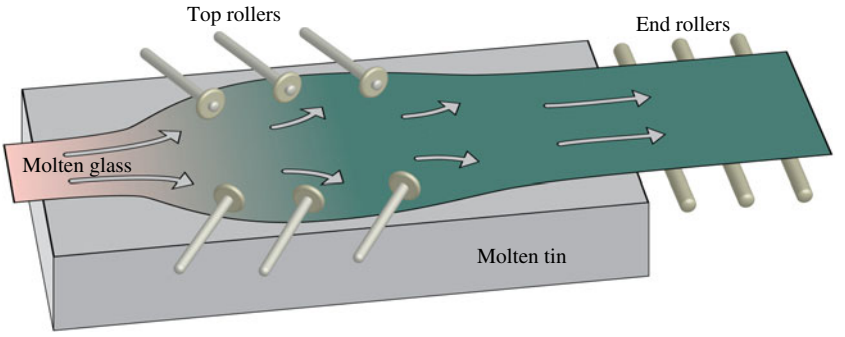


FIGURE 1. (Colour online available at journals.cambridge.org/flm) Principle of the float glass process: molten glass floats on top of molten tin. While it cools down, the glass is stretched by top rollers and end rollers to achieve the desired thickness. The float part is about 50 m long and 10 m wide.

Thin viscous sheet models have also been used to model the large-scale deformation of continents (England & McKenzie 1983) and the buckling of oceanic lithosphere during subduction (Guillou-Frottier, Buttles & Olson 1995; Ribe *et al.* 2007).

On the time scales of organismal growth, cells and tissues can be considered as viscous bodies. For instance, the growth of plant cells has been investigated using models of inflated anisotropic viscous shells (Dyson & Jensen 2010). At the supra-cellular level, a growing tissue is compressed by neighbouring tissues with a lower growth rate. As a consequence, buckling instabilities can also be expected, yielding a mechanism for morphogenesis, as for organogenesis in plants (Steele 2000) or fingerprint formation (Kücken & Newell 2004), or convolutions of the brain (Toro & Burnod 2005). We note, however, that, except in this last study, models were built upon purely elastic approaches.

In the glass industry, thin sheets are given prescribed shapes and thickness by applying mechanical forcing while they cool down (Pearson 1985). In the second part of this paper we will consider the case study of a floating sheet, which is motivated by both plate tectonics and glass industry. The glass float process (Pilkington 1969) is used for a continuous production of thin glass (figure 1). At one end of a long bath of liquid tin, molten glass is poured from the furnace and spreads out forming a layer of floating glass (tin is denser than glass), cooling down as it gets farther from the furnace. In order to make the layer thinner than the capillary length, a set of rollers are used to stretch the floating sheet, which comes out solidified at the other end of the bath, after it has undergone a transverse compression. The corresponding compressive stress may induce buckling.

Taylor (1968) demonstrated the buckling of viscous threads and sheets in various experimental geometries. His work was inspired by the Rayleigh–Stokes analogy (Stokes 1845; Rayleigh 1896), according to which the Stokes equations for a viscous fluid are similar to the equations for the equilibrium of a Hookean (linearly elastic) incompressible solid, with the fluid velocity and viscosity replaced by the solid displacement and one-third the Young's modulus, respectively.

The seminal paper of Taylor (1968) inspired a number of subsequent studies. He first showed that a viscous thread can buckle under longitudinal compression, an instability that was investigated theoretically by Buckmaster, Nachman & Ting (1975) and Buckmaster & Nachman (1978). Taylor also repeated Barnes & Woodcock's 1958

https://doi.org/10.1017/jfm.2011.256 Published online by Cambridge University Press

experiment on the coiling of a viscous jet impinging on a wall. In this geometry, buckling is triggered by the reaction force of the wall (see e.g. Cruickshank & Munson 1982; Mahadevan, Ryu & Samuel 1998). These and other phenomena have been further investigated, and we refer the reader to Marheineke & Wegener (2009) for a review on viscous threads and jets.

Taylor (1968) also demonstrated buckling in a sheared annular layer of viscous liquid floating on an inviscid bath, and proposed a qualitative interpretation: shear stress induces compression at 45° from the annulus midline. This experiment was repeated by Suleiman & Munson (1981), who investigated quantitatively the critical shear rate for buckling, and the wavelength of the undulations. They identified the relevant dimensionless groups but failed to predict the critical mode and its threshold. This problem was again considered by Benjamin & Mullin (1988), who obtained a quantitative agreement with the experiments, based on a stability analysis of the three-dimensional viscous flow. This instability is controlled by external forces (gravity and surface tension), and is essentially a buckling instability. An analysis based on the equations for thin viscous sheets was still lacking; one is proposed here as an application of our generic equations. A variant of the annular buckling experiment was proposed by Blake & Bejan (1984), who considered a rectangular floating sheet in contact with a container along three edges, and compressed along the fourth edge which is moving inwards.

The buckling of thin viscous sheets can also be induced by body forces. For instance, when an air bubble rising in a viscous liquid reaches the surface, a thin film of liquid separates it from ambient air. When this film is punctured, the air trapped in the bubble escapes; the hole grows while the viscous film falls under its own weight and makes wrinkles in the azimuthal direction (Debrégeas, de Gennes & Brochard-Wyart 1998; Da Silveira, Chaïeb & Mahadevan 2000). The same phenomenon occurs when a very viscous sheet drapes a stick (Boudaoud & Chaïeb 2001). In both cases, a semi-quantitative analysis taking advantage of the analogy between viscous and elastic sheets showed that gravity generates a compressive stress in the plane tangent to the sheet, while the most unstable mode is selected by a balance between gravity and viscous forces. Finally, the gravity-driven drawing of glass or polymer sheets can generate stress in the sheet and induce buckling (Filippov & Zheng 2010).

Most of the theoretical work on viscous sheets has relied on dimensional reduction. Indeed, asymptotic expansions in the limit of a small ratio between thickness and longitudinal length scale enable the derivation of governing equations for the dynamics of the mid-surface. Compared to the full, three-dimensional equations (e.g. Benjamin & Mullin 1988), dimensional reduction retains only the relevant modes of stretching and bending and can make more advanced analyses possible, such as exploring the nonlinear regime; it also eases numerical simulations. Dimensionally reduced models have been derived under specific assumptions: by Buckmaster *et al.* (1975) and Ribe (2001) for two-dimensional problems (planar threads and cylindrical sheets); for axisymmetric three-dimensional problems where bending is dominated by stretching (Pearson & Petrie 1970*a*,*b*; Yarin, Gospodinov & Roussinov 1994); for non-axisymmetric, three-dimensional problems where bending is dominated by stretching (van de Fliert, Howell & Ockendon 1995), with applications to the drawing of a tube (Griffiths & Howell 2007, 2008, 2009) and of a flat sheet (Scheid *et al.* 2009; Filippov & Zheng 2010). Bending effects have only been considered by Howell (1996) in the case of nearly flat sheets and by Ribe (2002) for general shapes.

https://doi.org/10.1017/jfm.2011.256 Published online by Cambridge University Press

In this paper, we investigate the dynamics of nearly flat sheets. The closest work in the literature is that of Howell (1996) and Ribe (2002). Our approach is to derive the various limit models in a unified way, to consider arbitrary external forces (thereby extending Howell's results), and derive the equations in a form that is suited to stability analyses. Ribe considers finite rotations and the resulting equations are fairly general, except that external forces in the bulk are assumed to be constant. Our equations, being based on the small slope approximation, are compact and perfectly suited to the linear and nonlinear stability analyses of floating viscous sheets. We use formal asymptotic expansions to deduce the equations for thin sheets from the equations for three-dimensional viscous fluids, building on previous work done in the context of elastic plates such as the classical paper of Ciarlet (1980).

In § 2 we derive two limit models depending on the magnitude of external loading. The full set of equations governing the thin sheet in three dimensions are given in § 2.4. The analysis of stability of a floating sheet is prepared in § 3: the general equations for thin viscous sheets are specified to the case of a floating sheet subjected to gravity, buoyancy and surface tension (§ 3.1); an unperturbed solution is defined (§ 3.2) and a linearization near this solution is introduced (§ 3.3). The linear stability of a floating sheet is investigated in § 4 at short times, and in § 5 at long times. An amplitude equation characterizing the nonlinear buckling amplitude is derived in § 4.2. In § 6 we discuss the range of validity of our analysis and provide orders of magnitude relevant to applications.

2. Derivation of the models

We start by deriving a set of dimensionally reduced equations for thin viscous sheets, which are used in the stability analyses in the second part of the paper. In § 2.1, we formulate the problem in two dimensions and introduce some useful notation. In § 2.2, the equations for the balance of momentum in the fluid are expanded with respect to the small aspect ratio – thickness to typical longitudinal length – allowing integration across the thickness and yielding equilibrium equations for the stress resultants and torques at different orders. These equations of equilibrium are combined with the constitutive law for a Newtonian viscous fluid in § 2.3. In § 2.4, the assumption of a two-dimensional flow is relaxed. Readers not interested in the details can skip ahead to this last subsection, § 2.4, where the equations governing the dynamics of viscous sheets subjected to external forces are summarized.

2.1. *Equilibrium equations in the two-dimensional case*

Cartesian coordinates (x, y, z) are chosen such that the sheet lies in the (x, y) plane in undeformed state. We start with a two-dimensional formulation, assuming invariance with respect to the y direction. At any time t, let $z = H(x, t)$ be the position of the centre-surface of the sheet, and let $h(x, t)$ be its thickness. All variables, including forces, may depend on time; however, this dependence will be implicit to make notation more concise (the variable t is often omitted). The equations of the interfaces are

$$z_\pm(x, t) = H(x, t) \pm \frac{h(x, t)}{2}, \tag{2.1}$$

where the '+' is for the upper interface, and the '−' for the lower one. Let $\boldsymbol{n}_\pm(x, t)$ and $\boldsymbol{t}_\pm(x)$ denote the unit normals and tangents at either interface, with the orientation chosen as in figure 2. Both volume and surface forces may be applied on the sheet. These forces are collectively represented by a volume distribution of force $\boldsymbol{f}(x, z, t)$:

https://doi.org/10.1017/jfm.2011.256 Published online by Cambridge University Press

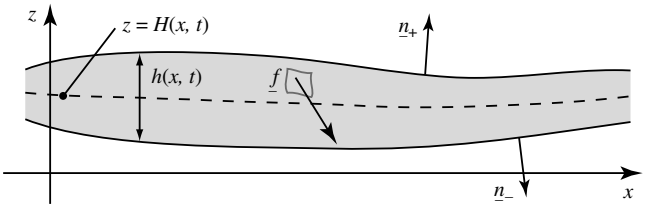


FIGURE 2. Cross-section of a viscous sheet in the plane (x, z) in a two-dimensional geometry.

surface forces such as surface tension are taken care of by a Dirac contribution to the volume force $\boldsymbol{f}$. We consider the limit of a small Reynolds number $\rho UL/\mu$ (μ being the fluid dynamic viscosity) and neglect inertial terms in the equations of equilibrium. Equilibrium in the bulk and along the interfaces read, in terms of the Cauchy stress tensor $\boldsymbol{S}$:

$$\boldsymbol{\nabla} \cdot \boldsymbol{S}(x, z) + \boldsymbol{f}(x, z) = \boldsymbol{0} \quad \text{for } z_-(x) \leqslant z \leqslant z_+(x), \tag{2.2a}$$

$$\boldsymbol{S}(x, z_\pm(x)) \cdot \boldsymbol{n}_\pm(x) = 0. \tag{2.2b}$$

Let us introduce some mathematical operators acting on a vertical slice of fluid. They will help us keep notation concise while dealing with arbitrary distributions of forces across the thickness. Given some function $\phi(x, z)$, defined in the volume occupied by the sheet, we first define its thickness integral, and its first and second moments:

$$[I \cdot \phi](x) = \int_{z_-(x)}^{z_+(x)} \phi(x, z)\, \mathrm{d}z, \tag{2.3a}$$

$$[J \cdot \phi](x) = \int_{z_-(x)}^{z_+(x)} (z - H(x))\phi(x, z)\, \mathrm{d}z, \tag{2.3b}$$

$$[K \cdot \phi](x) = \int_{z_-(x)}^{z_+(x)} \frac{(z - H(x))^2}{2}\phi(x, z)\, \mathrm{d}z. \tag{2.3c}$$

These operators will be useful for projecting the three-dimensional forces into effective forces for the two-dimensional model: see equations (2.43*a*) and (2.43*b*). In addition, the following two operators will be useful in the intermediate steps of the calculation:

$$[A \cdot \phi](x, z) = \int_{H(x)}^{z} \phi(x, z')\, \mathrm{d}z', \tag{2.3d}$$

$$[\chi \cdot \phi](x) = \int_{z_-(x)}^{z_+(x)} k_\chi(x, z)\phi(x, z)\, \mathrm{d}z, \tag{2.3e}$$

where the kernel is defined by

$$k_\chi(x, z) = \begin{cases} +1/2 & \text{if } H(x) < z < z_+(x), \\ -1/2 & \text{if } z_-(x) < z < H(x). \end{cases} \tag{2.3f}$$

Note that the result of all these operators is a function of the sole variable x, except for the 'indefinite' integral operator $[A \cdot \phi](x, z)$, which retains an additional dependence on the transverse coordinate z. The operators listed here satisfy useful identities derived in Appendix A.

https://doi.org/10.1017/jfm.2011.256 Published online by Cambridge University Press

2.2. *Expansion at different orders*

The model is derived by expansion with respect to the small aspect ratio ϵ,

$$\epsilon = \frac{z^*}{L}, \tag{2.4}$$

where z^* is the typical value of the sheet thickness $h(x)$, and L is a typical in-plane length. The in-plane coordinate x is rescaled using L:

$$x = L\tilde{x}, \tag{2.5a}$$

where tilde is used for the rescaled variables. In contrast, the transverse coordinate z, thickness, and deflection of the centre-surface $H(x)$ are rescaled using $z^* = \epsilon L$:

$$z = \epsilon L\tilde{z}, \tag{2.5b}$$

$$h(x) = \epsilon L\tilde{h}(\tilde{x}), \tag{2.5c}$$

$$H(x) = \epsilon L\tilde{H}(\tilde{x}). \tag{2.5d}$$

The rescaled interface position $\tilde{z}_\pm(\tilde{x})$ is defined using (2.1) as

$$\tilde{z}_\pm(\tilde{x}) = (1/\epsilon L)z_\pm(x) = \tilde{H}(\tilde{x}) \pm (\tilde{h}(\tilde{x})/2). \tag{2.6}$$

The upper and lower interfaces have small slope, and the unit normal there, to order one in ϵ, is given by

$$\boldsymbol{n}_\pm(\tilde{x}) = \begin{pmatrix} \mp\epsilon\tilde{z}_{\pm,\tilde{x}}(\tilde{x}) \\ \pm 1 \end{pmatrix}. \tag{2.7}$$

Here and elsewhere we use the notation $\phi_{,s} = \partial\phi/\partial s$ for the partial derivative of a function ϕ with respect to the variable s.

We consider the following rescaling and expansion for the internal stress $\boldsymbol{S}$,

$$S_{xx}(x, z) = \frac{\mu U}{L}(\epsilon^0\tilde{S}^{(0)}_{xx}(\tilde{x}, \tilde{z}) + \cdots), \tag{2.8a}$$

$$S_{xz}(x, z) = \frac{\mu U}{L}(\epsilon\tilde{S}^{(1)}_{xz}(\tilde{x}, \tilde{z}) + \cdots), \tag{2.8b}$$

$$S_{zz}(x, z) = \frac{\mu U}{L}(\epsilon^0\tilde{S}^{(0)}_{zz}(\tilde{x}, \tilde{z}) + \epsilon^2\tilde{S}^{(2)}_{zz}(\tilde{x}, \tilde{z}) + \cdots), \tag{2.8c}$$

where ellipses denote higher-order terms. The overall factor $\mu U/L$ has been introduced by anticipating the viscous constitutive law, U being defined later as the typical in-plane velocity. For all terms but $\tilde{S}^{(0)}_{zz}$, the proposed hierarchy of powers of ϵ on the right-hand sides follows from a balance of the stress gradients $S_{ij,j}$ arising in the divergence in (2.2*a*); note that spatial derivatives scale differently along the in-plane and out-of-plane directions, namely $\partial/\partial x \sim \epsilon^0$ and $\partial/\partial z \sim 1/\epsilon$. The additional term $\tilde{S}^{(0)}_{zz}$ of order ϵ^0 is required because of the constitutive relation of the fluid. The pressure required to ensure incompressibility forces the orthogonal components S_{xx} and S_{zz} to have the same leading order with respect to ϵ (see (2.22*a*) and (2.41)); even if the fluid were compressible, the components S_{xx} and S_{zz} would still be coupled, as both depend linearly on the components xx and yy of the strain-rate tensor.

Substituting these scalings for the stress into the balance of forces (2.2*a*), we find that the net internal force $\boldsymbol{\nabla}\cdot\boldsymbol{S}$ is of order one along the x axis, and has contributions of order $1/\epsilon$ and ϵ along the z axis; consistency dictates the following scaling for the

https://doi.org/10.1017/jfm.2011.256 Published online by Cambridge University Press

applied forces (density per unit volume):

$$f_x(x,z) = \frac{\mu U}{L^2}(\tilde{f}_x^{(0)}(\tilde{x},\tilde{z}) + \cdots), \tag{2.9a}$$

$$f_z(x,z) = \frac{\mu U}{L^2}\left(\frac{1}{\epsilon}\tilde{f}_z^{(-1)}(\tilde{x},\tilde{z}) + \epsilon\tilde{f}_z^{(1)}(\tilde{x},\tilde{z}) + \cdots\right). \tag{2.9b}$$

Here, f_x and f_z denote the projections of the force $\boldsymbol{f}$ onto the x and z directions: $\boldsymbol{f}(x,z) = (f_x(x,z), 0, f_z(x,z))$. We have been led naturally to assume different scaling assumptions for the in-plane and out-of-plane components of the force in the presence of a slender geometry.

To avoid cumbersome notation, tildes will be dropped in the remainder of this section: we shall always deal with rescaled quantities, unless specified otherwise.

We proceed to plug these expansions into the general equations for a two-dimensional viscous fluid. Let us start with the equilibrium (2.2*a*), considered at order zero along the x direction, and at orders both (-1) and 1 along the z direction:

$$S_{xx,x}^{(0)}(x,z) + S_{xz,z}^{(1)}(x,z) + f_x^{(0)}(x,z) = 0, \tag{2.10a}$$

$$S_{zz,z}^{(0)}(x,z) + f_z^{(-1)}(x,z) = 0, \tag{2.10b}$$

$$S_{zz,z}^{(2)}(x,z) + S_{xz,x}^{(1)}(x,z) + f_z^{(1)}(x,z) = 0. \tag{2.10c}$$

Regarding the consistency with respect to the parameter ϵ, recall that z is a first-order quantity and so $\partial/\partial z$ is of order $1/\epsilon$; as a result, the term $S_{xz,z}^{(1)}$ for instance is of order $\epsilon/\epsilon = \epsilon^0$, and so is consistent with the other terms in the first equation.

Similarly, by equation (2.2*b*), the continuity of stress at the interfaces at order one along the x direction and at orders zero and two along the z direction is given by

$$-z_{\pm,x}(x)S_{xx}^{(0)}(x,z_\pm(x)) + S_{xz}^{(1)}(x,z_\pm(x)) = 0, \tag{2.11a}$$

$$S_{zz}^{(0)}(x,z_\pm(x)) = 0, \tag{2.11b}$$

$$-z_{\pm,x}(x)S_{xz}^{(1)}(x,z_\pm(x)) + S_{zz}^{(2)}(x,z_\pm(x)) = 0. \tag{2.11c}$$

A solvability condition for $S_{zz}^{(0)}$ (also known as a Fredholm alternative) can be found by integrating the left-hand side of (2.10*b*) with respect to z and inserting the boundary conditions (2.11*b*) into $\int_{z_-}^{z_+} S_{zz,z}^{(0)}\,\mathrm{d}z = S_{zz}^{(0)}(x,z_+) - S_{zz}^{(0)}(x,z_-)$. This yields $\int_{z_-}^{z_+} f_z^{(-1)}\,\mathrm{d}z = 0$ or, in concise notation,

$$[I \cdot f_z^{(-1)}](x) = 0. \tag{2.12}$$

This equation implies a balance of transverse forces at dominant order, $f_z^{(-1)}$. An equation for the balance of transverse forces at second order, $f_z^{(1)}$, will be derived later by pushing the expansion further; see (2.20).

The axial balance at first order is found by integration of (2.10*a*) with respect to z : $[I \cdot (S_{xx,x}^{(0)})] + [I \cdot (S_{xz,z}^{(1)})] + [I \cdot f_x^{(0)}] = 0$. Using the identities (A 1) and (A 2), derived in Appendix A, to rewrite the first and second terms, we have

$$\left(\frac{\mathrm{d}[I \cdot S_{xx}^{(0)}]}{\mathrm{d}x} - (z_+)_{,x}S_{xx}^{(0)+} + (z_-)_{,x}S_{xx}^{(0)-}\right) + (S_{xz+}^{(1)} - S_{xz-}^{(1)}) + [I \cdot f_x^{(0)}] = 0, \tag{2.13}$$

where $S_{\alpha\beta}^{(i)\pm}$ is a shorthand notation for $S_{\alpha\beta}^{(i)}(x,z_\pm(x))$. By (2.11*a*), four terms cancel out in this equation and we have

$$N_{xx,x}(x) + [I \cdot f_x^{(0)}](x) = 0, \tag{2.14}$$

https://doi.org/10.1017/jfm.2011.256 Published online by Cambridge University Press

where we have introduced the membrane stress N_{ij}, also known as the internal stress resultant:

$$N_{ij}(x,t) = [I \cdot S^{(0)}_{ij}](x,t). \tag{2.15}$$

Equation (2.14) is a balance of longitudinal forces, the first term coming from internal stress, the second one from applied forces.

We push the expansion further to obtain the transverse balance at the next order. Integration of (2.10*c*) with respect to z yields $[I \cdot (S^{(1)}_{xz,x})] + [I \cdot (S^{(2)}_{zz,z})] + [I \cdot f^{(1)}_z] = 0$. Repeating a similar calculation as that leading to (2.14), but now using the other boundary condition (2.11*c*), we end up with

$$[I \cdot S^{(1)}_{xz}]_{,x}(x) + [I \cdot f^{(1)}_z](x) = 0. \tag{2.16}$$

This equation still depends on a secondary quantity, $S^{(1)}_{xz}$, and needs more work.

To eliminate the shear stress $S^{(1)}_{xz}$, let us apply the moment operator J defined by (2.3*b*) on both sides of (2.10*a*):

$$[J \cdot (S^{(0)}_{xx,x})] + [J \cdot (S^{(1)}_{xz,z})] + [J \cdot f^{(0)}_x] = 0. \tag{2.17}$$

The first term of this equation is rewritten using the identity (A 5) with $\gamma = S^{(0)}_{xx}$ (integration by parts along the x direction), and the second term using the other identity (A 6) with $\gamma = S^{(1)}_{xz}$ (integration by parts along the z direction). This yields

$$\left([J \cdot S^{(0)}_{xx}]_{,x} + H_{,x}[I \cdot S^{(0)}_{xx}] - \frac{h(x)}{2}(z_{+,x}S^{(0)+}_{xx} + z_{-,x}S^{(0)-}_{xx})\right) \cdots$$
$$+ \left(-[I \cdot S^{(1)}_{xz}] + \frac{h(x)}{2}(S^{(1)+}_{xz} + S^{(1)-}_{xz})\right) + [J \cdot f^{(0)}_x] = 0. \tag{2.18}$$

By the boundary condition (2.11*a*), all terms proportional to $h(x)$ cancel out. Solving for the resultant of the shear stress, also known as the internal normal force, we find

$$[I \cdot S^{(1)}_{xz}](x) = [J \cdot S^{(0)}_{xx}]_{,x}(x) + H_{,x}[I \cdot S^{(0)}_{xx}](x) + [J \cdot f^{(0)}_x](x). \tag{2.19}$$

Substituting this into (2.16), we finally obtain the balance of transverse forces at second order in compact form,

$$M_{xx,xx}(x) + (H_{,x}N_{xx})_{,x}(x) + [J \cdot f^{(0)}_x]_{,x}(x) + [I \cdot f^{(1)}_z](x) = 0, \tag{2.20}$$

where we have introduced the bending moment M_{ij}, defined by

$$M_{ij}(x,t) = [J \cdot S^{(0)}_{ij}](x,t). \tag{2.21}$$

Equation (2.20) complements the balance of transverse forces at dominant order zero, obtained earlier in (2.12). While the equation at dominant order was uncoupled to the dynamics of the sheet, the new equation (2.20) couples the viscous stress M_{xx} and N_{xx} to the applied force $f^{(0)}_x$ and $f^{(1)}_z$.

These equations are interpreted in Appendix B.

2.3. *Combining with viscous constitutive law*

The equations of equilibrium derived so far are valid for any thin sheet in the small-slope approximation. We shall now introduce the constitutive law for an incompressible, purely viscous Newtonian fluid with uniform dynamic viscosity μ; the case of thin sheets with non-uniform viscosity across thickness is considered in a different paper by the same authors (Pfingstag, Audoly & Boudaoud 2011). Let $\boldsymbol{u}(x,z)$

https://doi.org/10.1017/jfm.2011.256 Published online by Cambridge University Press

be the velocity in the fluid. Conservation of volume and Stokes' law read, returning temporarily to non-scaled variables,

$$\boldsymbol{\nabla} \cdot \boldsymbol{u}(x, z) = 0, \tag{2.22a}$$

$$\boldsymbol{S}(x, z) = -p(x, z)\mathbf{1} + 2\mu \boldsymbol{D}(x, z), \tag{2.22b}$$

where the strain-rate tensor $\boldsymbol{D}(x, z)$ is the symmetric part of the gradient of velocity. The components of the velocity are denoted by

$$\boldsymbol{u}(x, z) = (u(x, z), 0, w(x, z)). \tag{2.23}$$

The second component along the y axis is set to zero since we assume a two-dimensional flow for the moment, but this assumption will be relaxed later. There should be no confusion between the vector $\boldsymbol{u}$ and its x component, denoted by u.

At the interfaces, one more set of conditions involving the velocities is required in order to ensure kinematic compatibility:

$$w(x, z_\pm(x)) = z_{\pm,t}(x) + z_{\pm,x}(x)u(x, z_\pm(x)). \tag{2.24}$$

We consider additional scaling assumptions, which complement those given at the beginning of § 2.2. We first use the constitutive law (2.22*b*) to rescale the pressure and strain rate consistently with (2.7):

$$\boldsymbol{D}(x, z) = \frac{U}{L}\tilde{\boldsymbol{D}}(\tilde{x}, z), \tag{2.25a}$$

$$p(x, y) = \frac{\mu U}{L}\tilde{p}(\tilde{x}, \tilde{z}). \tag{2.25b}$$

We introduced earlier the quantity U, defined as the typical in-plane velocity: we shall therefore assume that the expansion for $u(x, z)$ is of the form

$$u(x, z) = U(\tilde{u}^{(0)}(\tilde{x}, \tilde{z}) + \cdots), \tag{2.25c}$$

where the ellipsis stands again for higher-order terms.

We also need to specify how time and transverse velocity scale with ϵ. Two different sets of scaling can be considered, as in the work of Howell (1996), namely the Trouton scaling and the BNT scaling. Here BNT stands for Buckmaster, Nachman and Ting who first introduced this scaling (Buckmaster *et al.* 1975; Buckmaster & Nachman 1978). The Trouton scaling assumes $t \sim L/U$ and $w = \epsilon U$, while the BNT scaling assumes $t \sim \epsilon^2 L/U$ and $w = \epsilon^{-1}U$. We recall here that since inertia has been neglected, time only appears in the kinematic equation (2.24), which describes the evolution of the sheet geometry. As will become apparent in the reduced equations for the sheet, the Trouton scaling is more elementary and corresponds to a deformation dominated by the stretching of the sheet, while the BNT scaling accounts for both stretching and bending. Both cases are taken care of by the notation

$$t = \epsilon^{2m}\frac{L}{U}\tilde{t}, \tag{2.26a}$$

$$w(x, z) = \epsilon^{1-2m}U(\tilde{w}^{(1-2m)}(\tilde{x}, \tilde{z}) + \cdots). \tag{2.26b}$$

Value of the index m is defined to be 0 in the Trouton case, and 1 in the BNT case:

$$m = \begin{cases} 0 & \text{(Trouton)}, \\ 1 & \text{(BNT)}, \end{cases} \qquad (1-m) = \begin{cases} 1 & \text{(Trouton)}, \\ 0 & \text{(BNT)}. \end{cases} \tag{2.26c}$$

https://doi.org/10.1017/jfm.2011.256 Published online by Cambridge University Press

We shall use the 'reciprocal' indices m and $(1-m)$ routinely as a means to track terms that are present with BNT scaling only, or with Trouton scaling only. Since m is only allowed to take on values 0 or 1, the following identity will be used later to simplify some expressions:

$$m(1-m)=0. \tag{2.27}$$

In what follows, we shall again drop tildes for the sake of readability: we deal implicitly with rescaled quantities, unless specified otherwise.

2.3.1. *Solving for the velocity field*

Let us consider the strain-rate tensor $\boldsymbol{D}(x,z)$. The axial strain $D_{xx}=u^{(0)}_{,x}(x,z)+\cdots$ is a quantity of order ϵ^0 with our rescaling; transverse strain $D_{zz}=\epsilon^{-2m}w^{(1-2m)}_{,z}(x,z)+\cdots$ is a quantity of order ϵ^{-2m}, that is of order ϵ^0 in the Trouton case ($m=0$) and of order ϵ^{-2} in the BNT case. In both cases, the incompressibility condition (2.22*a*) requires that the equation $D_{xx}+D_{zz}=0$ holds to leading order, ϵ^{-2m}: we have $w^{(1)}_{,z}+u^{(0)}_{,x}=0$ in the Trouton case, or $w^{(-1)}_{,z}=0$ in the BNT case. In concise notation, we have

$$w^{(1-2m)}_{,z}(x,z)+(1-m)u^{(0)}_{,x}(x,z)=0. \tag{2.28a}$$

Consider now the shear strain rate, $D_{xy}(x,z)=1/2(u_{,z}+w_{,x})$. Its leading order, which is formally ϵ^{-1} in both the Trouton and BNT cases, has to cancel in order for the shear stress S_{xz} to remain of order ϵ as implied by (2.8*b*), and not ϵ^{-1}. The condition $u_{,z}+w_{,x}=0$ yields $u^{(0)}_{,z}=0$ in the Trouton case, and $u^{(0)}_{,z}+w^{(-1)}_{,x}=0$ in the BNT case, which we summarize as

$$u^{(0)}_{,z}(x,z)+mw^{(1-2m)}_{,x}(x,z)=0. \tag{2.28b}$$

Substitution of (2.28*b*) into the derivative of (2.28*a*) with respect to z yields, with the help of the identity (2.27), $w^{(1-2m)}_{,zz}(x,z)=0$. A similar equation can be derived by substituting (2.28*a*) into the derivative of (2.28*b*) with respect to z. This yields

$$u^{(0)}_{,zz}(x,z)=0, \quad w^{(1-2m)}_{,zz}(x,z)=0. \tag{2.29}$$

This implies that both $u^{(0)}(x,z)$ and $w^{(1-2m)}(x,z)$ depend linearly on z: for some functions $\overline{u}(x)$, $\overline{w}(x)$, $\breve{u}(x)$ and $\breve{w}(x)$ depending on x (and implicitly on time t) but not on z, we have

$$u^{(0)}(x,z)=\breve{u}(x)(z-H(x))+\overline{u}(x), \tag{2.30}$$

$$w^{(1-2m)}(x,z)=\breve{w}(x)(z-H(x))+\overline{w}(x). \tag{2.31}$$

The functions $\breve{u}(x)$ and $\breve{w}(x)$ can be found by substituting into (2.27): $\breve{u}(x)=-m\overline{w}_{,x}(x)$ and $\breve{w}(x)=-(1-m)\overline{u}_{,x}(x)$. We have just determined the leading orders of the axial and transverse velocities u and w, up to two functions $\overline{u}(x)$ and $\overline{w}(x)$ that do not depend on z:

$$u^{(0)}(x,z)=-m\overline{w}_{,x}(x)(z-H(x))+\overline{u}(x), \tag{2.32a}$$

$$w^{(1-2m)}(x,z)=-(1-m)\overline{u}_{,x}(x)(z-H(x))+\overline{w}(x). \tag{2.32b}$$

Let us now consider the kinematic compatibility condition (2.24), which we read off to leading order ϵ^{1-2m}:

$$w^{(1-2m)}(x,z_\pm(x))=z_{\pm,t}(x)+(1-m)z_{\pm,x}(x)u^{(0)}(x,z_\pm(x)). \tag{2.33}$$

Note that the last term, of order ϵ, is not visible at order $\epsilon^{1-2m}=\epsilon^{-1}$ when $m=1$, but is visible at order $\epsilon^{1-2m}=\epsilon$ when $m=0$, hence the prefactor $(1-m)$. Inserting

https://doi.org/10.1017/jfm.2011.256 Published online by Cambridge University Press

the definition of $z_\pm$ from (2.1) and the explicit form of $w^{(1-2m)}$ found in (2.32*b*), we have

$$-(1-m)\overline{u}_{,x}\left(\pm\frac{h}{2}\right)+\overline{w}=\left(H_{,t}\pm\frac{h_{,t}}{2}\right)+(1-m)\left(H_{,x}\pm\frac{h_{,x}}{2}\right)\overline{u}. \tag{2.34}$$

This equation has been simplified by dropping a term containing a factor $m(1-m)$, which is zero by (2.27). One condition holds on the upper interface (when replacing the symbol $\pm$ by $+$), and another condition holds on the lower interface (replacing $\pm$ by $-$). Considering the average of these two conditions (2.34), we find

$$\overline{w}(x)=H_{,t}(x)+(1-m)H_{,x}(x)\overline{u}(x). \tag{2.35}$$

When replaced into (2.32*a*), this yields an explicit solution for the in-plane velocity, after using (2.27) one more time:

$$u^{(0)}(x,z)=\overline{u}(x)-mH_{,xt}(z-H(x)). \tag{2.36}$$

In the Trouton case ($m=0$), the in-plane velocity $u^{(0)}$ appears to be independent of the transverse coordinate z; in the BNT case, the last term shows up, accounting for the kinematics of bending.

Considering now the difference of (2.34) from the lower interface to the upper one, we find

$$-(1-m)\overline{u}_{,x}(x)h(x)=h_{,t}+(1-m)h_{,x}(x)\overline{u}(x), \tag{2.37}$$

which can be put in a more compact form:

$$h_{,t}(x)+(1-m)(h(x)\overline{u}(x))_{,x}=0. \tag{2.38}$$

This is the conservation of volume integrated across the thickness: it reads $h_{,t}+(h\overline{u})_{,x}=0$ in the Trouton case; in the BNT case, we have simply $h_{,t}=0$.

2.3.2. *Solving for the in-plane stress*

Consider (2.10*b*) for transverse equilibrium at order ϵ^{-1}, namely $S^{(0)}_{zz,z}(x,z)+f_z^{(-1)}(x,z)=0$. The general solution of this differential equation for $S^{(0)}_{zz}$ can be expressed in terms of the operator A carrying out z integration and of a constant of integration $\overline{S}_{zz}(x)$ independent of z:

$$S^{(0)}_{zz}(x,z)=-[A\cdot f_z^{(-1)}](x,z)+\overline{S}_{zz}(x). \tag{2.39}$$

Substituting this into (2.11*b*), which expresses transverse equilibrium of the interface at order ϵ^0, we find $\overline{S}_{zz}(x)=[A\cdot f_z^{(-1)}](x,z_+(x))$ and $\overline{S}_{zz}(x)=[A\cdot f_z^{(-1)}](x,z_-(x))$. Taking the average of these equalities, and using identity (A 7), we find the constant of integration $\overline{S}_{zz}(x)=[\chi\cdot f_z^{(-1)}](x)$. Therefore,

$$S^{(0)}_{zz}(x,z)=-[A\cdot f_z^{(-1)}](x,z)+[\chi\cdot f_z^{(-1)}](x). \tag{2.40}$$

Finally, the constitutive law (2.22*b*) yields $S^{(0)}_{xx}(x,z)=2u^{(0)}_{,x}(x,z)-p(x,z)$ and $S^{(0)}_{zz}(x,z)=-2u^{(0)}_{,x}(x,z)-p(x,z)$: by the condition of incompressibility, $D_{zz}=-D_{xx}=-u^{(0)}_{,x}$. Eliminating the pressure, we find

$$S^{(0)}_{xx}(x,z)=4u^{(0)}_{,x}(x,z)+S^{(0)}_{zz}(x,z). \tag{2.41}$$

https://doi.org/10.1017/jfm.2011.256 Published online by Cambridge University Press

Substituting now our solution for $u^{(0)}(x,z)$ from (2.36), and our solution for $S^{(0)}_{zz}(x,z)$ from (2.40), we find an explicit solution for the in-plane stress:

$$S^{(0)}_{xx}(x,z) = 4\overline{u}_{,x}(x) - 4m(H_{,xt}(x)(z-H(x)))_{,x} - [A\cdot f_z^{(-1)}](x,z) + [\chi\cdot f_z^{(-1)}](x). \tag{2.42}$$

Again, note that the Trouton and BNT cases yield similar expressions, except for the bending term which is present only in the BNT theory.

By integration of (2.42) across thickness we can now compute the stress resultant N_{ij} and moment M_{ij} defined earlier in (2.15) and (2.21). Using the identities (A 8*a*) and (A 8*b*) and the transverse equilibrium in (2.12) to simplify the terms proportional to $f_z^{(-1)}$, we have

$$N_{xx}(x) = 4\mu h(x)(\overline{u}_{,x}(x) + mH_{,xt}(x)H_{,x}(x)) + [J\cdot f_z^{(-1)}](x), \tag{2.43a}$$

$$M_{xx}(x) = -m\frac{\mu h^3(x)}{3}H_{,xxt}(x) + [K\cdot f_z^{(-1)}](x). \tag{2.43b}$$

Note that the transverse force $f_z^{(-1)}$ appears in the expressions of the longitudinal stress resultant and moment; this contamination can be attributed to the coupling via the pressure. Even though its value is $\mu = 1$ in our choice of rescaled units, we have restored the viscosity μ in the above equations for improved readability.

2.4. *Generalization to three dimensions*

We recapitulate all the equations that govern the dynamics of the viscous sheet, which were obtained previously by expansion. In passing, we relax the assumption of invariance along the y direction (three-dimensional case); we shall not justify the derivation of the three-dimensional setting again, as it follows the same lines as the two-dimensional setting. The in-plane variables are now x and y; the in-plane components of the external force are denoted by $(f_x(x,y,z), f_y(x,y,z))$. We describe the evolution of the thickness $h(x,y,t)$ and height $H(x,y,t)$ of the sheet, and the in-plane average velocity $(\overline{u}(x,y,t), \overline{v}(x,y,t))$. As earlier, the Trouton and BNT models are gathered in a single set of equations, by introducing two indices $(1-m)$ and m: the Trouton model is recovered by setting $(1-m)=1$ and $m=0$, and the BNT model by $(1-m)=0$, $m=1$.

The following set of equations extends the equations of the previous section. Mass conservation (2.38) becomes

$$h_{,t}(x,y) + (1-m)\left(\frac{\partial(\overline{u}(x,y)h(x,y))}{\partial x} + \frac{\partial(\overline{v}(x,y)h(x,y))}{\partial y}\right) = 0. \tag{2.44}$$

The axial force balance (2.14) now reads

$$\begin{aligned} N_{xx,x}(x,y) + N_{xy,y}(x,y) &= -[I\cdot f_x^{(0)}](x,y), \\ N_{xy,x}(x,y) + N_{yy,y}(x,y) &= -[I\cdot f_y^{(0)}](x,y). \end{aligned} \tag{2.45}$$

The transverse balance of force at order zero reads, from (2.12),

$$[I\cdot f_z^{(-1)}] = 0, \tag{2.46a}$$

and order two, from (2.20),

$$\begin{aligned} &(M_{xx,xx} + 2M_{xy,xy} + M_{yy,yy}) + (N_{xx}H_{,xx} + 2N_{xy}H_{,xy} + N_{yy}H_{,yy}) \\ &\quad + (-H_{,x}[I\cdot f_x^{(0)}] - H_{,y}[I\cdot f_y^{(0)}] + [J\cdot f_x^{(0)}]_{,x} + [J\cdot f_y^{(0)}]_{,y}) + [I\cdot f_z^{(1)}] = 0. \end{aligned} \tag{2.46b}$$

https://doi.org/10.1017/jfm.2011.256 Published online by Cambridge University Press

Note that we have expanded the derivative in the second term in (2.20) here, and simplified using the in-plane equilibrium. The membrane stress N_{ij} and the internal moment M_{ij} are given by effective constitutive laws, which extend those given in (2.45):

$$\left.\begin{aligned} N_{xx}(x,y) &= 2\mu h(x,y)(2(\overline{u}_{,x}(x,y)+mH_{,xt}H_{,x})+(\overline{v}_{,y}(x,y)+mH_{,yt}H_{,y})) \\ &\quad +[J\cdot f_z^{(-1)}](x,y) \\ N_{xy}(x,y) &= \mu h(x,y)((\overline{u}_{,y}(x,y)+mH_{,xt}H_{,y})+(\overline{v}_{,x}(x,y)+mH_{,yt}H_{,x})), \\ N_{yy}(x,y) &= 2\mu h(x,y)((\overline{u}_{,x}(x,y)+mH_{,xt}H_{,x})+2(\overline{v}_{,y}(x,y)+mH_{,yt}H_{,y})) \\ &\quad +[J\cdot f_z^{(-1)}](x,y), \end{aligned}\right\} \tag{2.47}$$

$$\left.\begin{aligned} M_{xx}(x,y) &= -m\frac{\mu h^3(x,y)}{3}\left(H_{,xxt}+\frac{1}{2}H_{,yyt}\right)+[K\cdot f_z^{(-1)}](x,y), \\ M_{xy}(x,y) &= -m\frac{\mu h^3(x,y)}{3}\left(\frac{1}{2}H_{,xyt}\right), \\ M_{yy}(x,y) &= -m\frac{\mu h^3(x,y)}{3}\left(H_{,yyt}+\frac{1}{2}H_{,xxt}\right)+[K\cdot f_z^{(-1)}](x,y). \end{aligned}\right\} \tag{2.48}$$

Here the mean surface position H is a function of x, y and t. Equations (2.47) and (2.48) are written in compact form and justified in full detail in a follow-up paper by the same authors (Pfingstag *et al.* 2011).

2.5. *Discussion*

These equations generalize the results of Howell (1996) to arbitrary forces. The general equations of Ribe (2002) can be shown to be equivalent to the compact set of equations above in the case of small slope and constant bulk external forces. The order of magnitude of the transverse forces and the scaling for the time should now be chosen depending on the specific problem considered. Note that the order of magnitude U of the in-plane velocity can be set by the forcing applied along the boundaries, or by distributed in-plane forces f_x and f_y.

When transverse forces f_z are large compared to $\mu U/L^2$, they should be considered to be of order (-1) and assigned to the contribution $f_z^{(-1)}$; then the transverse balance is given by (2.46*a*), and (2.46*b*) can be discarded. In that case, the BNT scaling suppresses all time derivatives, indicating that the time scale considered is too short for the sheet to evolve. In contrast, the Trouton scaling corresponds to observing the sheet over a much longer time scale, where it does evolve. In such circumstances, Trouton scaling is appropriate and BNT scaling can be viewed as a degenerate case.

By contrast, when transverse forces f_z are small compared to $\mu U/L^2$, one should set $f_z^{(-1)}=0$, assign them to $f_z^{(1)}$ and use (2.46*b*) for the transverse balance of forces. Combined with Trouton scaling, this equation is singular in the presence of compressive stress: equation (2.46*b*) attempts to describe buckling but with a zero bending stiffness: with $m=0$ in (2.48), the bending rigidity appears to be zero in the Trouton case. This leads to spatial undulations with arbitrarily small wavelength, a phenomenon known as membrane wrinkling in the context of elastic plates and shells, see e.g. the work of Dret & Raoult (1995). Therefore, in the case of 'small' transverse forces, BNT scaling is more appropriate.

Note that we can combine the Trouton and BNT models into a single, hybrid model. The trick is (i) to re-sum, i.e. write the equations for $f_z=\epsilon^{-1}f_z^{(-1)}+\epsilon f_z^{(1)}+\cdots$ and not for $f_z^{(-1)}$ and $f_z^{(1)}$ separately: this has the effect of removing ϵ from the equations and

https://doi.org/10.1017/jfm.2011.256 Published online by Cambridge University Press

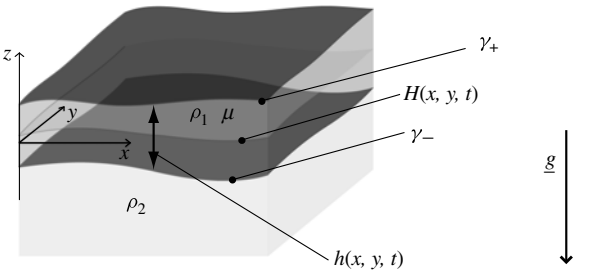


FIGURE 3. Geometry of a floating viscous sheet in a three-dimensional geometry.

there is no longer a need to keep track of the indices in parentheses for the order; (ii) to retain all terms that appear either in the Trouton or BNT model: we take $m = 0$ in (2.44),

$$h_{,t}(x, y) + \frac{\partial(\overline{u}(x, y)h(x, y))}{\partial x} + \frac{\partial(\overline{v}(x, y)h(x, y))}{\partial y} = 0, \tag{2.49}$$

$m = 1$ in the stress resultants (2.47) and moments (2.48),

$$\left.\begin{aligned} N_{xx}(x, y) &= 2\mu h(x, y)(2(\overline{u}_{,x}(x, y) + H_{,xt}H_{,x}) + (\overline{v}_{,y}(x, y) + H_{,yt}H_{,y})) \\ &\quad + [J \cdot f_z^{(-1)}](x, y), \\ N_{xy}(x, y) &= \mu h(x, y)((\overline{u}_{,y}(x, y) + H_{,xt}H_{,y}) + (\overline{v}_{,x}(x, y) + H_{,yt}H_{,x})), \\ N_{yy}(x, y) &= 2\mu h(x, y)((\overline{u}_{,x}(x, y) + H_{,xt}H_{,x}) + 2(\overline{v}_{,y}(x, y) + H_{,yt}H_{,y})) \\ &\quad + [J \cdot f_z^{(-1)}](x, y), \end{aligned}\right\} \tag{2.50}$$

$$\left.\begin{aligned} M_{xx}(x, y) &= -\frac{\mu h^3(x, y)}{3}\left(H_{,xxt} + \frac{1}{2}H_{,yyt}\right) + [K \cdot f_z^{(-1)}](x, y), \\ M_{xy}(x, y) &= -\frac{\mu h^3(x, y)}{3}\left(\frac{1}{2}H_{,xyt}\right), \\ M_{yy}(x, y) &= -\frac{\mu h^3(x, y)}{3}\left(H_{,yyt} + \frac{1}{2}H_{,xxt}\right) + [K \cdot f_z^{(-1)}](x, y). \end{aligned}\right\} \tag{2.51}$$

Then, the problem is governed by mass conservation (2.49), longitudinal force balance (2.45) and transverse force balance (2.46*b*), complemented with the stress resultants (2.50) and moments (2.51). The resulting hybrid model enjoys the following property: it boils down to either the Trouton or BNT model when the corresponding scaling assumptions are made. As such, it provides a formal unification of the two models, which can be convenient for setting up numerical simulations, for example.

3. Application to the stability of floating viscous sheets

3.1. *Case of a floating, three-dimensional sheet with gravity, buoyancy and surface tension*

In the remainder of this paper, we apply our equations to a specific geometry: a thin, viscous sheet floating on a bath at hydrostatic equilibrium, with surface tension at the lower and upper interfaces. Each of the surface tensions γ_+ and γ_- at the upper and lower interfaces are assumed to be uniform. An in-plane flow of typical velocity U is imposed in the sheet, e.g. through in-plane loading. The density of the sheet material ρ_1 is smaller than that of the bath ρ_2. Let $z = H^b$ be the height of the free surface of

https://doi.org/10.1017/jfm.2011.256 Published online by Cambridge University Press

the bath when the sheet is absent. The bath is an inviscid fluid at rest; the pressure in the bath is purely hydrostatic, $p = \rho_2 g(H^b - z)$, where g is the acceleration of gravity.

The weight per unit volume of the sheet is simply $(\rho_1 g)$. Let z^* be the typical vertical displacement of the interfaces, be it due to deformations of the initially planar mid-surface, or to variations of thickness. Surface forces applied at the interfaces come from hydrostatic pressure, of order $(\rho_2 g z^*)$, and capillary pressure, of order $(\gamma z^*/L^2)$. Here γ is the typical value of surface tension and L an characteristic in-plane length, such as the wrinkling wavelength, or a scale imposed by the in-plane flow. These surface forces can be compared to the typical viscous force per unit volume, $(\mu U/L^2)$, times the typical thickness z^*, using non-dimensional numbers. The Jeffreys number (Jeffreys 1925; O'Keefe 1969) compares gravity and viscosity:

$$Je = \frac{\rho g L^2}{\mu U}, \tag{3.1}$$

where ρ stands for the order of magnitude of any of the densities. Similarly, the inverse capillary number compares surface tension and viscosity:

$$1/Ca = \frac{\gamma}{\mu U}. \tag{3.2}$$

A number of models could be considered based on these ingredients. We focus here on the case where gravity and surface tension both need to be considered in addition to viscosity. This is the most interesting situation since we have two factors that can limit the instabilities and which are potentially in competition: one relevant to large wavelengths and the other one to small wavelengths. Specifically, we consider two cases.

(*a*) Both the Jeffreys Je and inverse capillary $1/Ca$ number are small; transverse forces should be considered of order ϵ. The argument of § 2.5 suggests that we then consider short times and use the BNT scaling. The expressions of the applied forces read

$$f_z^{(-1)} = 0, \tag{3.3}$$

$$f_z^{(1)} = -\rho_1 g + \delta_+(x,y,z)(\gamma_+)\kappa_+(x,y) + \delta_-(x,y,z) \times \left[(\gamma_-)\kappa_-(x,y) + \rho_2 g\left(H^b - H + \frac{h}{2}\right)\right], \tag{3.4}$$

$$f_x^{(0)} = 0, \tag{3.5}$$

$$f_y^{(0)} = 0, \tag{3.6}$$

where $\delta_\pm(x,y,z) = \delta(z - z_\pm(x,y))$ denote the Dirac distributions centred on an interface $z = z_\pm(x,y)$, used here to account for surface forces, namely the capillary force and the force arising from pressure in the bath. In addition, we have introduced the following notation for the curvature of the lower and upper interfaces:

$$\kappa_\pm(x,y) = \nabla^2 z_\pm(x,y) = \nabla^2\left(H(x,y) \pm \frac{h(x,y)}{2}\right). \tag{3.7}$$

We will refer to the case $Je \ll 1$, $1/Ca \ll 1$ and $t \sim (z^*)^2/(LU)$ as the BNT case.

(*b*) Alternatively, we consider the case where both the Jeffreys Je and inverse capillary $1/Ca$ numbers are large; transverse forces should be considered of order $1/\epsilon$, and are considered part of $f_z^{(-1)}$ in our equations. Since the slope of the sheet is of order ϵ, the projection of normal forces onto the (x,y) plane are of order ϵ^0, and enter

https://doi.org/10.1017/jfm.2011.256 Published online by Cambridge University Press

into $f_x^{(0)}$ and $f_y^{(0)}$:

$$f_z^{(-1)} = -\rho_1 g + \delta_+(x,y,z)(\gamma_+)\kappa_+(x,y) + \delta_-(x,y,z) \times \left[(\gamma_-)\kappa_-(x,y) + \rho_2 g\left(H^b - H + \frac{h}{2}\right)\right], \tag{3.8}$$

$$f_z^{(1)} = 0, \tag{3.9}$$

$$f_x^{(0)} = \left(H + \frac{h}{2}\right)_{,x}(\gamma_+)\kappa_+(x,y) - \left(H - \frac{h}{2}\right)_{,x} \times \left[(\gamma_-)\kappa_-(x,y) + \rho_2 g\left(H^b - H + \frac{h}{2}\right)\right], \tag{3.10}$$

$$f_y^{(0)} = \left(H + \frac{h}{2}\right)_{,y}(\gamma_+)\kappa_+(x,y) - \left(H - \frac{h}{2}\right)_{,y} \times \left[(\gamma_-)\kappa_-(x,y) + \rho_2 g\left(H^b - H + \frac{h}{2}\right)\right]. \tag{3.11}$$

As explained in § 2.5, these large forces are studied at long times and using the Trouton scaling. We will simply refer to the case $Je \gg 1$, $1/Ca \gg 1$ and $t \sim L/U$ as the Trouton case.

These external forces are substituted into (2.44), (2.45) and (2.45). We keep notation concise using the number $m = 0$ for the Trouton case and $m = 1$ for the BNT case. We obtain the following set of equations. First, mass conservation remains

$$h_{,t}(x,y) + (1-m)\left(\frac{\partial(\overline{u}(x,y)h(x,y))}{\partial x} + \frac{\partial(\overline{v}(x,y)h(x,y))}{\partial y}\right) = 0. \tag{3.12}$$

The in-plane force balance is obtained from (2.45), using the forces given in (3.11) and (3.6) integrated over thickness:

$$N_{xx,x} + N_{xy,y} = -(1-m)\left(H + \frac{h}{2}\right)_{,x}(\gamma_+)\kappa_+(x,y) + (1-m)\left(H - \frac{h}{2}\right)_{,x} \times \left[(\gamma_-)\kappa_-(x,y) + \rho_2 g\left(H^b - H + \frac{h}{2}\right)\right], \tag{3.13a}$$

$$N_{xy,x} + N_{yy,y} = -(1-m)\left(H + \frac{h}{2}\right)_{,y}(\gamma_+)\kappa_+(x,y) + (1-m)\left(H - \frac{h}{2}\right)_{,y} \times \left[(\gamma_-)\kappa_-(x,y) + \rho_2 g\left(H^b - H + \frac{h}{2}\right)\right]. \tag{3.13b}$$

Inserting the forces in (3.11) and (3.6) into (2.47), and carrying out evaluation of the slice-based operators, we find the membrane stress:

$$N_{xx}(x,y) = 2\mu h[2(\overline{u}_{,x} + mH_{,xt}H_{,x}) + \overline{v}_{,y} + mH_{,yt}H_{,y}] + (1-m)h\frac{\gamma_+}{2}\kappa_+(x,y) - (1-m)h\frac{\gamma_-}{2}\kappa_-(x,y) - (1-m)h\frac{\rho_2 g}{2}\left(H^b - H + \frac{h}{2}\right), \tag{3.14}$$

https://doi.org/10.1017/jfm.2011.256 Published online by Cambridge University Press

$$N_{xy}(x,y) = \mu h[\overline{u}_{,y} + mH_{,xt}H_{,y} + \overline{v}_{,x} + mH_{,yt}H_{,x}], \tag{3.15}$$

$$\begin{aligned} N_{yy}(x,y) = {} & 2\mu h[\overline{u}_{,x} + mH_{,xt}H_{,x} + 2(\overline{v}_{,y} + mH_{,yt}H_{,y})] \\ & + (1-m)h\frac{\gamma_+}{2}\kappa_+(x,y) - (1-m)h\frac{\gamma_-}{2}\kappa_-(x,y) \\ & - (1-m)h\frac{\rho_2 g}{2}\left(H^b - H + \frac{h}{2}\right). \end{aligned} \tag{3.16}$$

In the Trouton case, the out-of-plane force balance (2.46*a*) boils down to

$$-(\gamma_+)\kappa_+(x,y) - (\gamma_-)\kappa_-(x,y) - \rho_2 g\left(H^b - H + \frac{h}{2}\right) + \rho_1 g h = 0 \quad (m=0), \tag{3.17a}$$

which is a partial differential equation for h and H. In the BNT case, we note that $[K \cdot f_z^{(-1)}](x,y) = 0$: we substitute the remaining terms in the expressions (2.48) of the moment, namely $M_{\alpha\beta}(x,y) = -(\mu h^3/3)(H_{,\alpha\beta t} + H_{,\gamma\gamma t}\delta_{\alpha\beta})/2$, into the transverse balance (2.46*b*), which yields

$$\begin{aligned} & N_{xx}H_{,xx} + 2N_{xy}H_{,xy} + N_{yy}H_{,yy} \\ & \quad = \frac{\mu h^3}{3}(H_{,xxxxt} + 2H_{,xxyyt} + H_{,y^4t}) - (\gamma_+)\kappa_+(x,y) \\ & \quad - (\gamma_-)\kappa_-(x,y) - \rho_2 g\left(H^b - H + \frac{h}{2}\right) + \rho_1 g h \quad (m=1). \end{aligned} \tag{3.17b}$$

3.2. *Base state*

We consider a flat configuration, $H(x,y,t) = H_0(t)$ and $h(x,y,t) = h_0(t)$, which is spatially uniform but may evolve with time. The remainder of this paper is concerned with a local analysis of stability of this flat configuration. By 'local analysis', we mean that the typical scale of the in-plane flow is assumed to be much larger than the wavelength of the possibly unstable modes. The analysis is carried out over an intermediate length scale, where the strain rate $\boldsymbol{D}$ can be considered uniform.

An in-plane flow can be present in this flat state, and can be driven by forcing at the boundaries. In the remainder of the paper, our main goal is to compute the growth rate of unstable modes, depending on the properties of this flow. To start with, we consider an in-plane flow that does not depend on time. This assumption can easily be relaxed: our expressions for the growth rate C as a function of the steady flow parameters α and β yield without modification the instantaneous growth rate as a function of the current flow parameters in the case of a time-dependent flow. This idea is implemented in full detail in § 5; see (5.2) in particular.

Let us call α and β the principal values of the two-dimensional strain rate, ordered with the convention

$$\alpha < \beta. \tag{3.18}$$

By convention, the x and y axes are aligned with the associated principal directions. This makes the strain-rate tensor diagonal, $D_{xx} = \alpha$, $D_{xy} = 0$ and $D_{yy} = \beta$. With this choice of axes, the in-plane velocity is given by

$$\overline{u}_0(x,y) = \alpha x, \tag{3.19}$$

$$\overline{v}_0(x,y) = \beta y. \tag{3.20}$$

https://doi.org/10.1017/jfm.2011.256 Published online by Cambridge University Press

On the right-hand side, we have omitted constants of integration representing a steady rigid-body motion, which do not affect the stability. Note that indices in parentheses, such as (0) in (2.32*a*) refer to the order in the expansion with respect to the small aspect ratio. By contrast, indices without parentheses refer to the expansion associated with the analysis of stability: in equation above, $\overline{u}_0$ refers to the base solution, and $\overline{u}_1$, introduced next, refers to the perturbation (marginally stable mode).

Conservation of mass (3.12) reads, for our planar solution,

$$h_{0,t}(t) + (1-m)(\alpha+\beta)h_0(t) = 0. \tag{3.21}$$

In the Trouton case ($m = 0$), the second term is non-zero and the thickness $h_0(t)$ of the base flow must depend explicitly on time, except in the special case of a pure shear flow ($\alpha + \beta = 0$).

In the absence of interface curvature, the transverse equilibrium (3.17*a*) or (3.17*b*) imposes the following buoyancy condition:

$$H_0(t) = H^b - \left(\frac{\rho_1}{\rho_2} - \frac{1}{2}\right) h_0(t). \tag{3.22}$$

Being homogeneous by assumption, the base state satisfies the in-plane force balance (3.13) automatically. The membrane stress is given by the constitutive law (3.16), which reads, after substitution of (3.22),

$$N^0_{xx}(t) = 2\mu(2\alpha+\beta)h_0(t) - (1-m)\frac{\rho_1 g h_0^2(t)}{2}, \tag{3.23a}$$

$$N^0_{xy}(t) = 0, \tag{3.23b}$$

$$N^0_{yy}(t) = 2\mu(\alpha+2\beta)h_0(t) - (1-m)\frac{\rho_1 g h_0^2(t)}{2}. \tag{3.23c}$$

This unperturbed membrane stress will appear in the equations for the linear stability.

3.3. *Perturbation*

We seek solutions to (3.12)–(3.17) by perturbing this spatially homogeneous base state:

$$h(x,y,t) = h_0(t) + h_1(x,y,t), \tag{3.24a}$$

$$H(x,y,t) = H_0(t) + H_1(x,y,t), \tag{3.24b}$$

$$\overline{u}(x,y,t) = \alpha x + \overline{u}_1(x,y,t), \tag{3.24c}$$

$$\overline{v}(x,y,t) = \beta y + \overline{v}_1(x,y,t), \tag{3.24d}$$

where $h_0(t)$, $H_0(t)$, $\overline{u}_0 = \alpha x$ and $\overline{v}_0 = \beta y$ characterize the flat base state of the previous section, and $h_1(x,y,t)$, $H_1(x,y,t)$, $\overline{u}_1(x,y,t)$, $\overline{v}_1(x,y,t)$ stand for the perturbations to thickness, mid-surface, and velocity.

As an illustration, we consider the case where the in-plane velocity is imposed at the boundaries, which is far from the region of interest. In view of this, the perturbation to velocity should vanish at infinity:

$$\lim_{(x,y)\to\infty} \overline{u}_1(x,y) = 0, \tag{3.25}$$

$$\lim_{(x,y)\to\infty} \overline{v}_1(x,y) = 0. \tag{3.26}$$

The stability is investigated next. In § 4 we treat the BNT case and find that the most unstable modes are purely undulatory (thickness h remains constant); in § 5 we study the Trouton case, and find that the unstable modes couple thickness and height variations.

https://doi.org/10.1017/jfm.2011.256 Published online by Cambridge University Press

4. Small forces, short time: undulatory perturbation

In this section we study the linear stability of the flat configuration under the scaling assumptions (*a*) of § 3.1, namely the BNT case ($m = 1$) with small transverse forces and short time.

4.1. *Linear stability analysis*

By (3.12), the thickness remains unperturbed when $m = 1$:

$$h_1(x, y, t) = 0. \tag{4.1}$$

Physically, this means that perturbations to thickness become significant on time scales that are much larger than those considered in the BNT case.

In the constitutive equation for membrane stress (3.16) all the nonlinear terms relevant to BNT case, such as $H_{,x}H_{,xt}$, appear as second-order quantities. Reading off the equation to first order, we have

$$N^1_{xx}(x, y) = 2\mu h_0[2\overline{u}_{1,x}(x, y) + \overline{v}_{1,y}(x, y)], \tag{4.2}$$

$$N^1_{xy}(x, y) = \mu h_0[\overline{u}_{1,y}(x, y) + \overline{v}_{1,x}(x, y)], \tag{4.3}$$

$$N^1_{yy}(x, y) = 2\mu h_0[\overline{u}_{1,x}(x, y) + 2\overline{v}_{1,y}(x, y)]. \tag{4.4}$$

These quantities are subjected to the in-plane equilibrium conditions (3.13), which for $m = 1$ are homogeneous equations:

$$N^1_{xx,x}(x, y) + N^1_{xy,y}(x, y) = 0, \tag{4.5}$$

$$N^1_{xy,x}(x, y) + N^1_{yy,y}(x, y) = 0. \tag{4.6}$$

Together with the asymptotic conditions (3.26), these two equations (4.4) and (4.6) constitute a well-posed problem for the velocities $\overline{u}_1$ and $\overline{v}_1$, which is uncoupled from the transverse quantities h_1 and H_1 (this decoupling is classical in the analysis of buckling near flat configurations, and comes from the up–down symmetry). Note that the time derivatives $\overline{u}_{1,t}$ or $\overline{v}_{1,t}$ do not show up in the above set of equations. In fact, we recognize the equations of two-dimensional, linearized elasticity when $\overline{u}_1$ and $\overline{v}_1$ are identified with displacement, and μ with an elastic modulus. With this analogy, equations (3.26) impose clamping conditions at infinity; then we know that the only solution is the trivial one,

$$\overline{u}_1(x, y) = 0, \quad \overline{v}_1(x, y) = 0, \tag{4.7}$$

for all values of x and y. Under the present assumptions, unstable modes are purely transverse.

Upon linearization, the transverse force balance (3.17*b*) provides an equation for the deflection H_1, which is decoupled from in-plane flow:

$$h_0[2(2\alpha + \beta)H_{1,xx} + 2(\alpha + 2\beta)H_{1,yy}] = \frac{1}{3}h_0^3(H_{1,xxxxt} + 2H_{1,xxyyt} + H_{1,y^4t}) - \frac{\gamma_+ + \gamma_-}{\mu}(H_{1,xx} + H_{1,yy}) + \frac{\rho_2 g}{\mu}H_1. \tag{4.8}$$

Here, we have substituted for the unperturbed membrane stress in expressions (3.23), and have linearized the nonlinear terms using equalities such as $(N_{xx}H_{,xx})_1 = N^0_{xx}H_{1,xx}$, since $H_{0,xx} = 0$.

https://doi.org/10.1017/jfm.2011.256 Published online by Cambridge University Press

The coefficients in linear equation (4.8) are independent both of time and space, and we seek a solution of the form

$$H_1(x, y, t) = \hat{H}_1 \mathrm{e}^{C_\mathrm{u} t + \mathrm{i}\boldsymbol{k}\cdot\boldsymbol{x}}, \tag{4.9}$$

where $\hat{H}_1$ is a complex amplitude, C_u is the growth rate to be determined later, $\boldsymbol{k} = (k_x, k_y)$ is the spatial wavenumber, and $\boldsymbol{x} = (x, y)$ the in-plane coordinate. We seek the wavevector in cylindrical coordinates,

$$k_x = k\,\cos\,\theta, \quad k_y = k\,\sin\,\theta, \tag{4.10}$$

where $\theta = 0$ corresponds to $\boldsymbol{k}$ aligned with the x axis, i.e. with the smallest eigenvalue α of the shear-rate tensor $\boldsymbol{D}$.

Substituting the trial form (4.9) into (4.8), we find an expression for the growth rate

$$C_\mathrm{u}(k, \theta) = \frac{6}{(h_0 k)^2}\left[-\alpha(1 + \cos^2\theta) - \beta(1 + \sin^2\theta) - \frac{1}{(h_0 k)^2}\left(\frac{(\gamma_+ + \gamma_-)h_0 k^2 + \rho_2 g h_0}{2\mu}\right)\right]. \tag{4.11}$$

A positive growth rate corresponds to an instability. For a given base flow, the wavevector corresponding to the most unstable mode is found by maximizing $C_\mathrm{u}(k, \theta)$ with respect to k and θ. By a convention expressed by (3.18), we have $\alpha < \beta$; as a result, the maximum of C_u with respect to θ is always reached for $\theta = 0$. Then, the wavenumber $\boldsymbol{k}$ is aligned with the x axis, and the instability pattern is made of stripes perpendicular to the x axis: see the inset in figure 5. This orientation of the pattern is characteristic of a buckling phenomenon as the x axis is the direction of most vigorous contraction, in the sense that $-\alpha > -\beta$ by (3.18).

Setting $\theta = 0$ in the equation above yields

$$\tau C_\mathrm{u}(k, \theta = 0) = \frac{6}{(h_0 k)^2}\left[p - \frac{1}{2(h_0 k)^2}\right], \tag{4.12}$$

where we have introduced the characteristic times obtained by balancing viscous effects and gravity, τ, and viscous effects and surface tension, τ_2, the Bond number, $\mathscr{C}$, and the control parameter, p; those parameters are defined by

$$\tau = \frac{\mu}{\rho_2 g h_0}, \quad \tau_2 = \frac{h_0 \mu}{\gamma_+ + \gamma_-}, \quad \mathscr{C} = \frac{\tau_2}{\tau}, \quad p = -\tau(2\alpha + \beta) - \frac{1}{2\mathscr{C}}. \tag{4.13}$$

They are all fixed once the base state is prescribed.

Typical plots of the growth rate $C_\mathrm{u}(k, 0)$ given by (4.12) as a function of wavelength k are shown in figure 4. For $p < 0$, C_u is negative for any value of k and the planar base state is linearly stable. For $p > 0$, however, there is a range of unstable wavelengths; the maximal value of the growth rate C_u^{max} and the associated wavelength k_{max} satisfy the following relations:

$$\tau C_\mathrm{u}^{max} = 3p^2, \quad h_0 k_{max} = \frac{1}{p^{1/2}} \quad (p > 0). \tag{4.14}$$

That is, in physical units,

$$C_\mathrm{u}^{max} = \frac{3\mu}{\rho_2 g h_0}\left[-(2\alpha + \beta) - \frac{\gamma_+ + \gamma_-}{2h_0\mu}\right]^2, \tag{4.15}$$

https://doi.org/10.1017/jfm.2011.256 Published online by Cambridge University Press

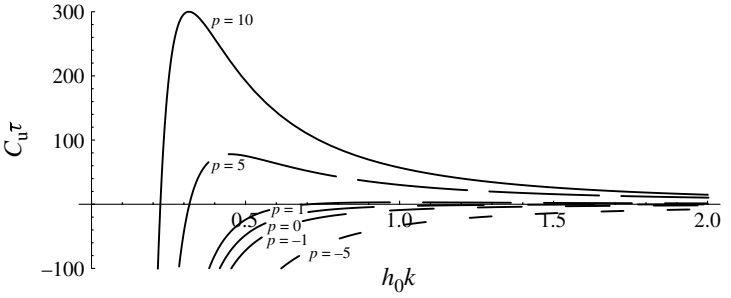


FIGURE 4. Dimensionless growth rate (τC_u) for the undulatory perturbation, plotted from (4.12) as a function of the dimensionless wavenumber ($h_0 k$). The most unstable direction $\theta = 0$ is considered.

$$k_{max} = \frac{\left(\dfrac{\rho_2 g}{h_0 \mu}\right)^{1/2}}{\left[-(2\alpha + \beta) - \dfrac{\gamma_+ + \gamma_-}{2h_0\mu}\right]^{1/2}}. \tag{4.16}$$

These expressions apply to the case $p > 0$, that is, when the argument of the square bracket is positive.

A stability diagram is plotted in figure 5 as a function of the flow properties. The curve corresponding to the loss of stability is given by the equation $p = 0$ for $\alpha < \beta$, and is thus a straight line in the upper-left part of the diagram. We complement the other half of the diagram, $\alpha > \beta$, by symmetry: in this region, the parameters α and β have to be swapped in the previous analysis to comply with (3.18). The angular point in the boundary corresponds to a change of orientation of the most unstable vector $\boldsymbol{k}$ by an angle $\pi/2$ when the principal values of the strain rate α and β cross each other. Note that the planar state is always stable when the flow is extensional along both its principal directions ($\alpha > 0$ and $\beta > 0$, implying $p < 0$). In the unstable regions, a buckling instability is driven by compressive membrane stress (when the flow is such that $\alpha < 0$ and/or $\beta < 0$), and resisted by buoyancy and surface tension: from (4.11), buoyancy is stabilizing at large values of the wavelength $2\pi/k$, while surface tension stabilizes relatively smaller wavelengths. As a result, the instability threshold depends on surface tension and buoyancy.

The thin-sheet approximation used here assumes that the wavelength is large compared to the thickness, $h_0 k \ll 1$. By (4.14), this requires that the parameter p is significantly larger than unity too. A limit case is when gravity vanishes, or when the compressive strain is high; the wavelength becomes large, and can even become comparable to the the lateral size of the system; the growth rate becomes large as well. This case corresponds to the observations of Taylor (1968) on compressed viscous threads, where the observed wavelength is comparable to the size of the object undergoing compression.

We also recover the results of the linear stability of Benjamin & Mullin (1988), who used the equations for volumetric viscous fluids (three dimensions) to interpret Taylor's experiment on the wrinkling of a sheared, floating annulus (Taylor 1968). The thin-sheet model used here makes the analysis considerably simpler, as there is no need to solve for the transverse dependence of the various quantities. We checked that the matrix in equation (28) obtained by Benjamin & Mullin (1988), assuming pure

https://doi.org/10.1017/jfm.2011.256 Published online by Cambridge University Press

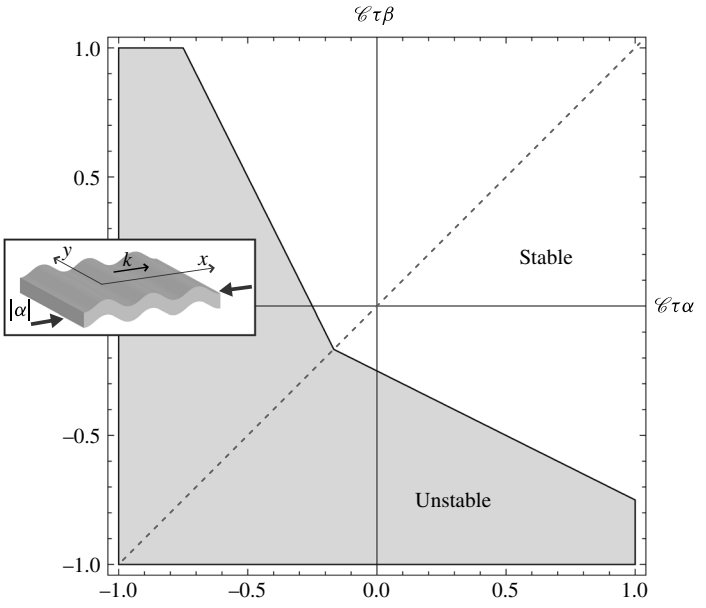


FIGURE 5. Stability with respect to buckling as a function of the principal values of strain rate (α, β), rescaled using the parameter $\tau_2 = \tau\mathscr{C}$. The buckling condition $p > 0$ defined in (4.14) has been rewritten as $2(\tau_2\alpha) + (\tau_2\beta) > -1/2$ using (4.13). This equation holds with the convention of axes defined in the main text, for which $\alpha < \beta$. The diagram has been extended below the dashed diagonal by mirror symmetry.

shear, yields our dispersion relation when expanded in the thin-sheet limit ($h_0 k \ll 1$) in the special case $\beta = -\alpha$ (pure shear).

In addition to providing a set of equations that can be readily applied to a variety of geometries, our framework can be used to address the nonlinear dynamics of thin sheets, as shown in the following section.

4.2. *Nonlinear stability analysis*

The linear stability analysis of the previous section predicts an exponential increase of the amplitude when the flow is unstable. For large amplitudes, linearization breaks down and a nonlinear analysis is required. The wavevector of the most unstable mode is along the x axis, which is by our orientation of axes the direction achieving the most vigorous contraction, see (3.18). We perform a nonlinear study of the most unstable mode, assuming that the invariance of the linear mode along the y direction carries on to the nonlinear regime,

$$H_{,y}(x, y, t) = 0, \quad N_{ij,y}(x, y, t) = 0, \quad \overline{u}_{,y}(x, y, t) = 0, \quad \overline{v}_{,y}(x, y, t) = 0, \tag{4.17}$$

where the in-plane indices i and j for N_{ij} can take on the values x or y. We seek the solutions H in the form (for the method, see e.g. Manneville 2004; Charru 2007)

$$H(x, t) = H_0(t) + \tfrac{1}{2}(A(t)\mathrm{e}^{\mathrm{i}k_{max}x} + A^*(t)\mathrm{e}^{-\mathrm{i}k_{max}x}), \tag{4.18}$$

where $A(t)$ is the complex amplitude of the pattern.

Before starting the calculation, we need to modify the asymptotic condition (3.26) for the in-plane velocity. Requiring convergence of velocity (u, v) to the reference flow $(\alpha x, \beta y)$ is appropriate at linear order, but not at second order. If imposed at second

https://doi.org/10.1017/jfm.2011.256 Published online by Cambridge University Press

order, it has the unwanted effect of suppressing the instability: by (4.25), growth of the cylindrical pattern is accompanied by a second-order in-plane velocity which is small and oscillatory, and does not converge to zero asymptotically for $(x, y) \to \infty$. To work around this, we require the following condition to hold at any time t:

$$\langle \overline{u}_{,x} \rangle_x(y) = \alpha \text{ for all } y, \quad \langle \overline{v}_{,y} \rangle_y(x) = \beta \text{ for all } x. \tag{4.19}$$

Here, $\langle f \rangle_x(y_0)$ denotes the average of a function $f(x, y)$ over the line with equation $y = y_0$, and its average $\langle f \rangle_x(x_0)$ over the line with equation $x = x_0$. Since (4.19) involves the averages of derivatives over an infinite domain, it is equivalent to the mild assumption that the difference between $\overline{u}(x, y)$ and αx, and between $\overline{v}(x, y)$ and βy, remains bounded. The aim of (4.19) is to prevent any systematic deviation from the reference solution $\overline{u} = \alpha x$ and $\overline{v} = \beta y$, and in this sense is in line with the former asymptotic condition (3.26).

Let us observe that the constitutive relations (3.16) for N_{xx} and N_{yy} can be solved for $u_{,x}$ and $v_{,y}$: with $m = 1$ and $H_{,y} = 0$, this yields

$$\overline{u}_{,x}(x, y, t) = \frac{2N_{xx}(x, y, t) - N_{yy}(x, y, t)}{6\mu h} - H_{,xt}(x, y, t)H_{,x}(x, y, t), \tag{4.20a}$$

$$\overline{v}_{,y}(x, y, t) = \frac{-N_{xx}(x, y, t) + 2N_{yy}(x, y, t)}{6\mu h}. \tag{4.20b}$$

By the invariance condition (4.17), all terms on the right-hand side of (4.20*b*) are actually independent of y, and so is $\overline{v}_{,y}$ too, $\overline{v}_{,y}(x, y) = \overline{v}_{,y}(x)$. This implies that averaging over y has no effect on $\overline{v}_{,y}$: $\langle \overline{v}_{,y} \rangle_y(x) = \overline{v}_{,y}(x)$. Combining with (4.19), we have

$$\overline{v}_{,y}(x, y, t) = \beta, \tag{4.21}$$

for any x, y and t: this component of the in-plane velocity remains unperturbed at all orders.

Substituting this expression into the constitutive equation (3.16) for N_{xx}, we have $(m = 1)$

$$N_{xx}(x, y, t) = 2\mu h(2\overline{u}_{,x} + \beta + 2H_{,xt}H_{,x}). \tag{4.22}$$

By the invariance (4.17), all terms in this equation are actually independent of y. Averaging over x, we obtain

$$\langle N_{xx} \rangle_x(t) = 2\mu h(2\alpha + \beta + 2\langle H_{,xt}H_{,x} \rangle_x(t)), \tag{4.23a}$$

after simplification of $\langle \overline{u}_{,x} \rangle_x$ using (4.19). Calculation of the average on the right-hand side is straightforward from (4.18):

$$\langle H_{,xt}H_{,x} \rangle_x(t) = +\frac{k_{max}^2}{2}|A(t)|\frac{\mathrm{d}|A(t)|}{\mathrm{d}t}. \tag{4.23b}$$

Using the invariance (4.17), the in-plane equilibrium condition (3.13*a*) boils down to $N_{xx,x}(x, y, t) = 0$, for $m = 1$: N_{xx} is independent of x, and we have

$$N_{xx}(x, y, t) = \langle N_{xx} \rangle_x(y, t). \tag{4.23c}$$

Combining the above three equations (4.22*a–c*), we find the value of the stress N_{xx}:

$$N_{xx}(x, y, t) = 2\mu h\left((2\alpha + \beta) + k_{max}^2|A(t)|\frac{\mathrm{d}|A(t)|}{\mathrm{d}t}\right), \tag{4.24}$$

https://doi.org/10.1017/jfm.2011.256 Published online by Cambridge University Press

a quantity which appears to be uniform in space. The last term in parentheses provides a nonlinear correction to the unperturbed membrane stress N^0_{xx} given in (3.23*a*).

The in-plane velocity $\overline{u}$ can be reconstructed from (4.22) by combining (4.18) and (4.24):

$$\overline{u}_{,x} = \alpha + \frac{k_{max}^2}{2}\left(\frac{A\dot{A}^* \mathrm{e}^{2\mathrm{i}k_{max}x} + \dot{A}A^* \mathrm{e}^{-2\mathrm{i}k_{max}x}}{2}\right). \tag{4.25}$$

As stated, this expression contains a constant part equal to the imposed average value, α, plus a second-order oscillatory part.

After dropping all terms involving some derivative along y, the transverse force balance (4.8) reads

$$\frac{\mu h^3}{3} H_{,xxxt} - (\gamma_+ + \gamma_-) H_{,xx} + \rho_2 g H = N_{xx} H_{,xx}. \tag{4.26}$$

We now substitute into this equation the expressions (4.18) for H and (4.24) for N_{xx}. This yields a differential equation for the evolution of the amplitude,

$$\begin{aligned}\frac{\mu h^3}{3} k_{max}^4 \frac{1}{A}\frac{\mathrm{d}|A(t)|}{\mathrm{d}t} + (\gamma_+ + \gamma_-)k_{max}^2 + \rho_2 g \\ = 2\mu h\left((2\alpha + \beta) + k_{max}^2 |A(t)| \frac{\mathrm{d}|A(t)|}{\mathrm{d}t}\right)(-k_{max}^2).\end{aligned} \tag{4.27}$$

Using the dimensionless parameters introduced in (4.13), this differential equation can be rewritten as

$$\frac{(hk_{max})^4}{6}\tau \frac{1}{A}\frac{\mathrm{d}|A(t)|}{\mathrm{d}t} = (hk_{max})^2 p - \frac{1}{2} - \frac{\tau (hk_{max})^4}{h^2}|A(t)|\frac{\mathrm{d}|A(t)|}{\mathrm{d}t}. \tag{4.28}$$

This expression can be simplified using the definitions of C_{u}^{max} and k_{max} in (4.14):

$$\frac{\mathrm{d}|A(t)|}{\mathrm{d}t} = C_{\mathrm{u}}^{max} A(t) - \frac{6}{h^2}|A(t)|\frac{\mathrm{d}|A(t)|}{\mathrm{d}t}A(t). \tag{4.29}$$

The exponential growth rate predicted by linear theory, $A_{,t} = C_{\mathrm{u}}^{max} A$, is recovered when the nonlinear term is omitted.

Since the complex argument of any solution $A(t)$ of (4.29) is conserved over time, $A(t)$ can be assumed to be real positive without loss of generality. The general solution of this equation is given by the following implicit equation:

$$\ln\frac{A(t)}{h} + 3\frac{A^2(t)}{h^2} = C_{\mathrm{u}}^{max}(t - t_0), \tag{4.30}$$

where t_0 is a constant of integration. This solution $A(t)$ is plotted in figure 6.

Equation (4.30) describes the transition from exponential growth $A(t) = A_0 \exp(C_{\mathrm{u}}^{max} t)$ at short times, to square-root growth $A(t) = h(C_{\mathrm{u}}^{max} t/3)^{1/2}$ at long times. The transition occurs when the amplitude reaches a value comparable to the thickness, $A/h \approx 1$, corresponding to $t - t_0 \sim 1/C_{\mathrm{u}}^{max}$. Note that the wavelength of the pattern, $2\pi/k_{max} \sim hp^{1/2}$, is much larger than the deflection h at the cross-over between the two regimes: using the small-slope approximation is consistent in the limit $|p| \gg 1$ considered here; it remains valid until time t becomes comparable to the large time p/C_{u}^{max}, which is when the amplitude of the pattern would become comparable to the wavelength.

https://doi.org/10.1017/jfm.2011.256 Published online by Cambridge University Press

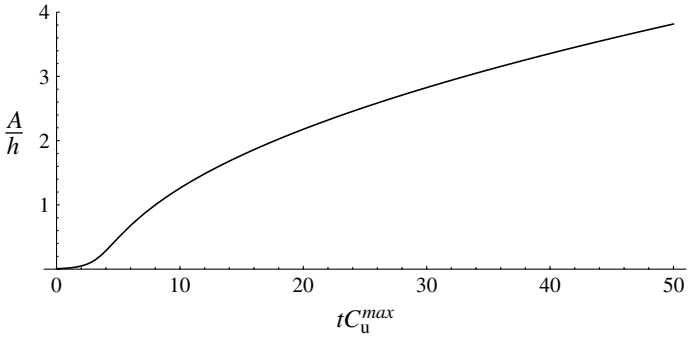


FIGURE 6. Time evolution of the amplitude of the undulatory mode predicted by the nonlinear analysis (4.30): dimensionless amplitude as a function of dimensionless time.

The square-root growth of the amplitude can be explained by the kinematics of inextensional wrinkling: the parenthesis on the right-hand side of (4.24) is the strain rate D_{xx}. For inextensional wrinkling, setting $D_{xx} = 0$ yields the scaling $A \sim t^{1/2}$. This square-root behaviour is also compatible with the nonlinear analysis of a thin viscous thread by Buckmaster *et al.* (1975).

We considered the pattern whose wavelength is fixed by the criterion of maximal growth rate in the framework of a linear stability analysis. A nonlinear analysis revealed that the exponential growth at short times predicted by linear theory is limited by nonlinear effects: when the deflection becomes comparable to the thickness of the sheet, the amplitude grows more slowly, like the square-root of time.

5. Large forces, long time: coupled perturbation

We study the stability of the planar solution given in § 3.2, and consider the Trouton case, that is, large transverse forces and long time. As before, we carry out a local stability analysis, and consider the in-plane velocity field $(\overline{u}_0, \overline{v}_0)$ given by (3.20), which depends linearly on the coordinates x and y. In the Trouton model, we can no longer ignore the evolution of thickness with time due to the two-dimensional divergence of the base flow: the solution of (3.21) is

$$h_0(t) = h_0(0)\mathrm{e}^{-(\alpha+\beta)t}. \tag{5.1}$$

Because of the explicit time dependence of the base solution (5.1), the simple exponential dependence assumed earlier in (4.9) is no longer applicable. We consider the more general form:

$$H_1(x, y, t) = \hat{H}_1 \mathrm{e}^{\Sigma(t)+\mathrm{i}\boldsymbol{k}(t)\cdot\boldsymbol{x}}, \tag{5.2a}$$

$$h_1(x, y, t) = \hat{h}_1 \mathrm{e}^{\Sigma(t)+\mathrm{i}\boldsymbol{k}(t)\cdot\boldsymbol{x}}, \tag{5.2b}$$

$$\overline{u}_1(x, y, t) = \mathrm{i}\hat{u}_1 \mathrm{e}^{\Sigma(t)+\mathrm{i}\boldsymbol{k}(t)\cdot\boldsymbol{x}}, \tag{5.2c}$$

$$\overline{v}_1(x, y, t) = \mathrm{i}\hat{v}_1 \mathrm{e}^{\Sigma(t)+\mathrm{i}\boldsymbol{k}(t)\cdot\boldsymbol{x}}, \tag{5.2d}$$

for the perturbed quantities H_1, h_1, $\overline{u}_1$ and $\overline{v}_1$ introduced in (3.24). The first term in the exponential is the integrated growth rate:

$$\Sigma(t) = \int_0^t C_{\mathrm{c}}(\tilde{t})\,\mathrm{d}\tilde{t}. \tag{5.2e}$$

https://doi.org/10.1017/jfm.2011.256 Published online by Cambridge University Press

We anticipate that the equation governing $C_c(t)$ is simpler than that for $\Sigma(t)$, and will eliminate Σ in favour of C_c whenever possible. Note that we have also kept an explicit dependence of the wavevector $\boldsymbol{k}(t)$ on time, for a reason that will soon be clear.

We can factor out the complex exponentials in (5.2) and introduce the following representation of the derivative operators:

$$\partial_t = C_c(t) + \mathrm{i}\boldsymbol{k}'(t)\cdot\boldsymbol{x}, \tag{5.3a}$$

$$\partial_x = \mathrm{i}k_x(t), \tag{5.3b}$$

$$\partial_y = \mathrm{i}k_y(t). \tag{5.3c}$$

Mass conservation (3.12) yields, at first order,

$$(C_c + \mathrm{i}\boldsymbol{k}'(t)\cdot\boldsymbol{x})\hat{h}_1 + (\alpha+\beta)\hat{h}_1 - h_0(k_x(t)\hat{u}_1 + k_y(t)\hat{v}_1) + \mathrm{i}(\overline{u}_0(x)k_x(t) + \overline{v}_0(y)k_y(t))\hat{h}_1 = 0. \tag{5.4}$$

Here we would have expected an algebraic equation for the amplitudes $\hat{h}_1$, $\hat{u}_1$ and $\hat{v}_1$, but find an additional dependence on the coordinates $\boldsymbol{x} = (x, y)$ through the terms $\boldsymbol{k}'(t)\cdot\boldsymbol{x}$, $\overline{u}_0(x) = \alpha x$ and $\overline{v}_0(y) = \beta y$. For this equation to be satisfied for any value of (x, y), we first require that the coefficients of x and y vanish. This yields $k_x'(t)+\alpha k_x = 0$ and $k_y'(t) + \beta k_y = 0$, which, in intrinsic variables, is given by

$$\frac{\partial \boldsymbol{k}(t)}{\partial t} = -\boldsymbol{D}(t)\cdot\boldsymbol{k}(t). \tag{5.5}$$

Equation (5.5) specifies the dilation and rotation of the wavenumber $\boldsymbol{k}(t)$ by the flow, and generalizes the one-dimensional derivation of Smith (1975). A similar equation has been used in combustion theory: in their equation (40), Zel'dovich *et al.* (1980) capture the effect of a velocity gradient on the growth rate of a harmonic perturbation advected along an expanding flame surface, which they call the stretch effect. We note that (5.5) can be interpreted as the conservation of the phase of the unstable mode by the co-moving derivative:

$$\left(\frac{\partial}{\partial t} + \overline{u}_0\frac{\partial}{\partial x} + \overline{v}_0\frac{\partial}{\partial y}\right)(\boldsymbol{k}(t)\cdot\boldsymbol{x}) = 0. \tag{5.6}$$

In this form, the equation appears to be related to the condition of advection of the phase of a WKB expansion in the analysis of short-scale perturbations in fluid mechanics; see, for instance, equation (7) of Lifschitz & Hameiri (1991).

When the advection condition (5.5) for the wavenumber is taken into account, the mass conservation (5.4) simplifies to

$$[C_c + \alpha + \beta]\hat{h}_1 + [-h_0(t)k_x(t)]\hat{u}_1 + [-h_0(t)k_y(t)]\hat{v}_1 = 0. \tag{5.7}$$

By the linearized balance of transverse force (3.17*a*), we have

$$\left[\rho_1 g - \frac{\rho_2 g}{2} + k^2(t)\frac{\gamma_+ - \gamma_-}{2}\right]\hat{h}_1 + [k^2(t)(\gamma_+ + \gamma_-) + \rho_2 g]\hat{H}_1 = 0. \tag{5.8}$$

To linear order, the in-plane force balance (3.13) yields

$$\mathrm{i}k_x\hat{N}^1_{xx} + \mathrm{i}k_y\hat{N}^1_{xy} = \rho_1 g h_0(t)(\mathrm{i}k_x(t))\left(\hat{H}_1 - \frac{\hat{h}_1}{2}\right), \tag{5.9a}$$

https://doi.org/10.1017/jfm.2011.256 Published online by Cambridge University Press

$$\mathrm{i}k_x\hat{N}^1_{xy} + \mathrm{i}k_y\hat{N}^1_{yy} = \rho_1 g h_0(t)(\mathrm{i}k_y(t))\left(\hat{H}_1 - \frac{\hat{h}_1}{2}\right), \tag{5.9b}$$

after simplifying the right-hand sides using the buoyancy condition (3.22). The linearized membrane stress $\hat{N}^1_{ij}$ is given by the constitutive relations (3.16):

$$\hat{N}^1_{xx} = h_0\left(-2\mu(2\hat{u}_1k_x + \hat{v}_1k_y) - \frac{(\gamma_+ - \gamma_-)}{2}k^2\hat{H}_1 - \frac{(\gamma_+ + \gamma_-)}{4}k^2\hat{h}_1 - \frac{\rho_2 g}{2}\left(-\hat{H}_1 + \frac{\hat{h}_1}{2}\right)\right) + \left(2\mu(2\alpha+\beta) - \frac{\rho_1 g h_0}{2}\right)\hat{h}_1, \tag{5.10a}$$

$$\hat{N}^1_{xy} = -\mu h_0(\hat{u}_1k_y + \hat{v}_1k_x), \tag{5.10b}$$

$$\hat{N}^1_{yy} = h_0\left(-2\mu(\hat{u}_1k_x + 2\hat{v}_1k_y) - \frac{(\gamma_+ - \gamma_-)}{2}k^2\hat{H}_1 - \frac{(\gamma_+ + \gamma_-)}{4}k^2\hat{h}_1 - \frac{\rho_2 g}{2}\left(-\hat{H}_1 + \frac{\hat{h}_1}{2}\right)\right) + \left(2\mu(\alpha+2\beta) - \frac{\rho_1 g h_0}{2}\right)\hat{h}_1. \tag{5.10c}$$

With the aim of formulating the stability problem in dimensionless form, we recall the characteristic times τ and τ_2 from (4.13), and introduce two new parameters τ_3 and τ_4:

$$\tau = \frac{\mu}{\rho_2 g h}, \quad \tau_2 = \frac{h\mu}{\gamma_+ + \gamma_-}, \quad \tau_3 = \frac{\mu}{(2\rho_1 - \rho_2)gh}, \quad \tau_4 = \frac{h\mu}{\gamma_+ - \gamma_-}. \tag{5.11}$$

Complementing $\mathscr{C} = \tau_2/\tau$ and p, we introduce another Bond number $\mathscr{C}_2 = \tau_4/\tau_3$, and the control parameter R:

$$\mathscr{C} = \frac{h^2\rho_2 g}{\gamma_+ + \gamma_-}, \quad \mathscr{C}_2 = \frac{h^2(2\rho_1 - \rho_2)g}{\gamma_+ - \gamma_-}, \quad R(\theta) = -\frac{\alpha\sin^2\theta + \beta\cos^2\theta}{2}. \tag{5.12}$$

The set of (5.7)–(5.10), after elimination of the membrane stress $\hat{N}_{ij}$, takes the form

$$\boldsymbol{M}\cdot\begin{pmatrix}\hat{h}_1\\ \hat{H}_1\\ \hat{u}_1\\ \hat{v}_1\end{pmatrix} = \begin{pmatrix}0\\0\\0\\0\end{pmatrix}, \tag{5.13}$$

$\boldsymbol{M}$ being defined by

$$\boldsymbol{M} = \begin{pmatrix} C_c + \alpha + \beta & 0 & -ckh_0 & -skh_0 \\ A_1 & 2A_2 & 0 & 0 \\ \left(2(2\alpha+\beta) - \frac{1}{4}A_2\right)c & -\frac{c}{2}A_1 & -h_0k(3c^2+1) & -3h_0ksc \\ \left(2(\alpha+2\beta) - \frac{1}{4}A_2\right)s & -\frac{s}{2}A_1 & -3h_0ksc & -h_0k(3s^2+1) \end{pmatrix}, \tag{5.14}$$

where $A_1 = (1/\tau_3) + (h_0^2k^2/\tau_4)$, $A_2 = (1/\tau) + (h_0^2k^2/\tau_2)$, $s = \sin\theta$ and $c = \cos\theta$, the angle θ between the x axis and the wavevector $\boldsymbol{k}(t)$ being defined in (4.10).

https://doi.org/10.1017/jfm.2011.256 Published online by Cambridge University Press

The existence of a solution to the linearized equations (5.13) requires the determinant of $\boldsymbol{M}$ to vanish. This condition yields an equation for the growth rate $C_c(k,\theta)$:

$$\tau C_c(k,\theta) = \tau R(\theta) + \frac{1}{16}\left[\left(\frac{\tau}{\tau_3}\right)^2 \frac{\left(1+\dfrac{(hk)^2}{\mathscr{C}_2}\right)^2}{1+\dfrac{(hk)^2}{\mathscr{C}}} - \left(1+\frac{(hk)^2}{\mathscr{C}}\right)\right]. \tag{5.15}$$

The case of pure shear flow ($\alpha = -\beta$) has been studied by Benjamin & Mullin (1988); for this type of flow, the above value of the growth factor C_c can be recovered from the matrix defined in their equation (28) in the thin-sheet limit ($hk \ll 1$). The set of equations presented here are valid for an arbitrary base flow.

The growth factor C_c is of variable sign depending on the value of the parameters. The first term on the right-hand side, proportional to $R(\theta)$, describes the effect of the in-plane flow, and is destabilizing for contractile flows. The first term in the square bracket is destabilizing and originates in the coupling between the two faces of the sheet. The second term (-1) in the square bracket describes the stabilization of all wavelengths by gravity, while the last term in the square bracket, proportional to $(hk)^2/\mathscr{C}$, accounts for the stabilization by surface tension, which is effective for short wavelengths.

With our convention $\alpha < \beta$, the growth factor C_c is maximal when the wavevector $\boldsymbol{k}$ is aligned with the y axis, that is, $\theta = \pi/2$. Indeed, this maximizes the only term depending on θ, namely $\tau R(\theta)$, by (5.12). In the absence of external forces, i.e. for a free-standing sheet, the square bracket cancels and the planar flow becomes unstable as soon as there exists a contractile direction in the base flow ($\alpha < 0$, $R(\pi/2) > 0$).

In figures 7 and 8, we have restored the external forces, but consider the particular case $\gamma_+ = \gamma_-$ and $\rho_2 = \rho_1$, for which

$$\frac{\tau}{\tau_3} = 1, \quad \frac{1}{\mathscr{C}_2} = 0. \tag{5.16}$$

In that case, (5.15) yields $\tau C_c(k,\theta) = \tau R(\theta) + (\breve{k}^{-1} - \breve{k})/16$ with $\breve{k} = 1 + (hk)^2/\mathscr{C} \geqslant 1$. The maximum with respect to the wavenumber is reached for $\breve{k} = 1$, that is, $k = 0$; the maximum with respect to the direction is reached for $\theta = \pi/2$. The stability is therefore determined by the sign of

$$\tau C_c\left(k = 0, \theta = \frac{\pi}{2}\right) = \tau R\left(\frac{\pi}{2}\right) = -\frac{\alpha\tau}{2}. \tag{5.17}$$

This yields the stability diagram above the dashed diagonal in figure 7. As earlier, the plot is extended below the diagonal by symmetry.

Figure 8 shows typical plots of the function $C_c(k,\pi/2)$ for various values on the parameters. Again we study the case defined by (5.16). Since the growth rate is plotted for $\theta = \pi/2$, it does not depend on the second flow parameter β, as long as $\beta > \alpha$. Varying the other flow parameter α can drive the system from stable to unstable state. The effect of the relative weight of gravity and surface tension is also illustrated in the figure. Unlike the buckling instability of § 4, this instability produces wrinkles oriented along, and not perpendicular to, the direction achieving largest contraction, which is the x direction with our choice of axes.

The sign of the second derivative of $C_c(k,\pi/2)$ at $k = 0$ is given by the sign of $[(\gamma_+ - \gamma_-)(\rho_1 - 2\rho_2)]$. When $[(\gamma_+ - \gamma_-)(\rho_1 - 2\rho_2)] < 0$, the function $C_c(k,\pi/2)$ has a

https://doi.org/10.1017/jfm.2011.256 Published online by Cambridge University Press

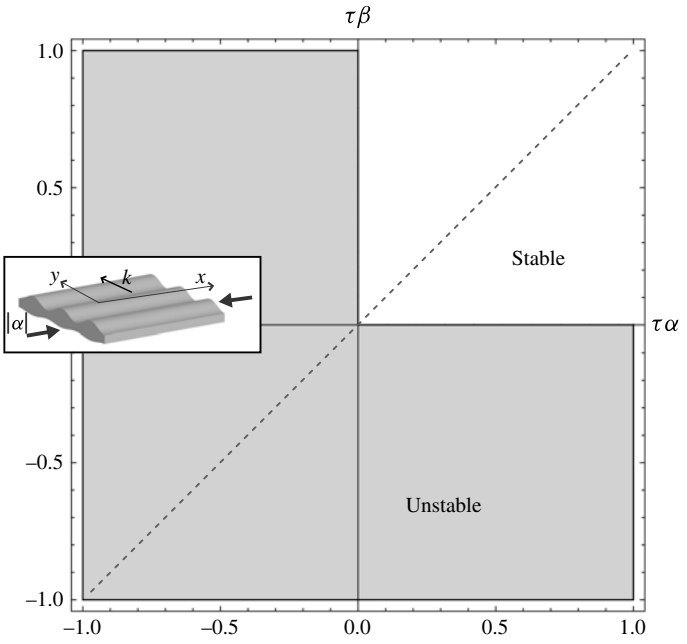


FIGURE 7. Stability with respect to coupled perturbations involving both thickness modulation and deflection of the mid-surface, as determined by the sign of $C_c(k = 0, \theta = \pi/2)$ in (5.17): phase diagram in the plane of the principal values of strain rate (α, β), rescaled using the time scale τ imposed by gravity and viscosity and defined in (5.11). Equation (5.17) holds above the diagonal ($\alpha < \beta$), the lower part of the diagram being obtained by symmetry.

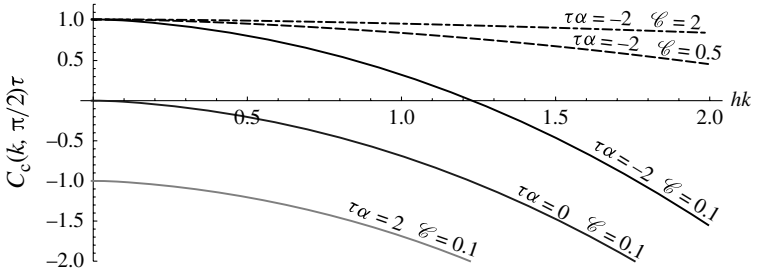


FIGURE 8. Dimensionless growth rate τC_c for the coupled perturbation, obtained by combining (5.15) and (5.16), as a function of the dimensionless wavenumber hk. Here, τ is a gravity–viscosity time scale, h is the thickness of the sheet, $\mathscr{C}$ is the Bond number defined in (5.11) and α is the most negative (contractile) principal strain rate. The value $\theta = \pi/2$ corresponds to the orientation of the most unstable mode. Note that for this particular value of θ, C_c does not depend on the flow parameter β.

maximum at $k = 0$ and the value of growth factor there determines the stability of the flow:

$$C_c^{max} = C_c\left(0, \frac{\pi}{2}\right) = -\frac{1}{2}\left(\alpha + \frac{1}{8\tau}\right) + \frac{\tau}{16\tau_3^2}. \tag{5.18}$$

https://doi.org/10.1017/jfm.2011.256 Published online by Cambridge University Press

When $[(\gamma_+ - \gamma_-)(\rho_1 - 2\rho_2)] < 0$ and $C_c^{max} > 0$, there is a range of unstable wavelengths. Large wavelengths are the most unstable ($k = 0$), and as a result the instability depends on the details of the boundary conditions at large scale and on the size of the system. This goes beyond the scope of the present analysis, which focuses on local buckling; still, the analysis of these global modes can be performed using the same set of dimensionally reduced equations, taking the appropriate boundary conditions into account.

6. Discussion

6.1. *A simplified hybrid model for reconciling the BNT and Trouton buckling analyses*

In § 4, an undulatory mode of instability has been found to occur using the BNT model. This model is relevant to short times, much shorter than the characteristic time $1/|\alpha| \sim 1/|\beta|$ of the base flow. This buckling mode is made up of stripes perpendicular to the most contractile direction ($\theta = 0$). In the limit of a free-standing viscous sheet, i.e. when capillary and buoyancy forces become negligible, this instability occurs whenever $(2\alpha + \beta) < 0$, as revealed by setting $\mathscr{C} = 0$ in (4.13). By (3.23*a*), this corresponds to existence of a compressive membrane stress N^0_{xx} along this most contractile direction x. Then the most unstable mode has infinite wavelength. All these features are characteristic of a buckling instability.

In § 5, the Trouton model was used. It is based on different scaling assumptions, and in particular is valid for much longer times, comparable to $1/|\alpha| \sim 1/|\beta|$. We found a different buckling mode, coupling thickness variations and undulations of the centre-surface, and with stripes now parallel to the most contractile direction ($\theta = \pi/2$).

This raises the question of whether these two modes can be in competition, or are a manifestation of a similar phenomenon viewed in two different limits. To answer this question, we propose a hybrid model that reconciles both analyses. This model is formal and simplified, and makes no claims to detailed accuracy. Its only goal is to provide a unified description of the two buckling modes. It is similar to the hybrid model of § 2.5, with the additional approximation that perturbations to the in-plane flow are neglected. Assuming $\overline{u}_1(x, y, t) = 0$ and $\overline{v}_1(x, y, t) = 0$ for any value of (x, y, t) is consistent with the solution for the undulatory mode, and changes quantitatively, but not qualitatively, the behaviour of the coupled mode.

Formally, the conservation of mass (3.21) at linear order yields $h_{1,t} + (\alpha + \beta)h_1 = 0$. We introduce a growth rate $C = \partial_t$ which is yet unknown, and rewrite this in the hybrid model as

$$(C + \alpha + \beta)\hat{h}_1 = 0. \tag{6.1}$$

We shall soon show that this equation is consistent with the two forms of the conservation of mass given earlier in the BNT and Trouton buckling analysis, when the two corresponding limits are considered.

We now consider out-of-plane equilibrium. Noting that the Trouton form (3.17*b*) of this equilibrium is a degenerate version of its BNT form (3.17*a*), we use the latter in the hybrid model. We linearize (3.17*a*) with respect to the perturbation (h_1, H_1). Symbolically, this yields

$$-N_0 k^2 \hat{H}_1 = \mu {h_0}^3 C k^4 \hat{H}_1 + (2A_2 \hat{H}_1 + A_1 \hat{h}_1). \tag{6.2}$$

Here, the coefficient N_0 represents the pre-stress in the base flow, given in (3.23), which provides the driving force for the buckling instability. The first term on the

https://doi.org/10.1017/jfm.2011.256 Published online by Cambridge University Press

right-hand side of (6.2) is the bending term. The last term represents the coupling of undulations ($\hat{H}_1$) and thickness variations ($\hat{h}_1$) through buoyancy and surface tension; this coupling is described by the coefficients A_1 and A_2, which were worked out in the Trouton analysis: see below (5.14). Their expressions are similar in the BNT case but we do not need to spell them out here. We shall soon check that the pre-stress and bending terms in (6.2) are negligible if the Trouton scaling assumptions are used, as expected.

Equations (6.1) and (6.2) can be combined in matrix form:

$$\boldsymbol{M}\cdot\begin{pmatrix}\hat{h}_1\\ \hat{H}_1\end{pmatrix}=\boldsymbol{0},\quad \text{where } \boldsymbol{M}=\begin{pmatrix}C+\alpha+\beta & 0\\ A_1 & \left(2A_2+N_0k^2+C\mu{h_0}^3k^4\right)\end{pmatrix}. \tag{6.3}$$

The growth rate is found by requiring that the determinant $\det \boldsymbol{M}=M_{11}M_{22}$ vanishes. One root corresponds to the vanishing of M_{11}, and describes a coupled mode,

$$C=C'_{\mathrm{c}},\quad \text{where } C'_{\mathrm{c}}=-(\alpha+\beta),\quad A_1\hat{h}_1^{\mathrm{c}}+(2A_2+\cdots)\hat{H}_1^{\mathrm{c}}=0, \tag{6.4a}$$

and the other one corresponds to the vanishing of M_{22}, an undulatory mode,

$$C=C'_{\mathrm{u}},\quad \text{where } C'_{\mathrm{u}}=\frac{1}{(h_0k)^2}\left(-\frac{N_0}{\mu h_0}-\frac{1}{(h_0k)^2}\frac{2A_2h_0}{\mu}\right),\quad \hat{h}_1\mathrm{u}=0. \tag{6.4b}$$

The hybrid model features both a coupled mode and an undulatory mode, and brings the BNT and Trouton analyses into a common framework. Note the close similarity of the expression for $\boldsymbol{M}$ in (6.3), above, with the upper-left block of the matrix $\boldsymbol{M}$ given earlier in (5.14) in the Trouton analysis; the detailed expressions of C_{c} and C'_{c} are different as the hybrid model ignores the perturbation to the in-plane flow. Note also that, formally, the expression (6.4*b*) for the growth rate C'_{u} of the undulatory mode in the approximate hybrid model, and the expression C_{u} coming from the BNT analysis (4.11) are identical.

From the hybrid model, the Trouton and BNT limits can be recovered by analysing the orders of magnitude of the growth rates C'_{u} and C'_{c} given above. Let us first introduce the typical time T_{f} associated with the base flow:

$$T_{\mathrm{f}}\sim\alpha^{-1}\sim\beta^{-1}\sim\frac{L}{U}. \tag{6.5}$$

We use the notation of § 2 for the orders of magnitude, namely U for in-plane velocity, L for the in-plane length, and ϵ for the aspect ratio h/L. The two growth rates appear to be vastly different:

$$C'_{\mathrm{u}}\sim\frac{N_0}{\mu{h_0}^3k^2}\sim\frac{\mu h_0\dfrac{U}{L}}{\mu{h_0}^3\dfrac{1}{L^2}}\sim\frac{1}{\epsilon^2T_{\mathrm{f}}},\quad C'_{\mathrm{c}}\sim\alpha\sim\beta\sim\frac{1}{T_{\mathrm{f}}}. \tag{6.6}$$

The typical growth time of the undulatory mode is $1/C'_{\mathrm{u}}\sim\epsilon^2T_{\mathrm{f}}$, which is precisely the short time scale of the BNT model ($m=1$) introduced earlier in (2.26*a*). The typical growth time of the coupled mode is $1/C'_{\mathrm{c}}\sim T_{\mathrm{f}}$, which is the time scale of the Trouton model ($m=0$) in (2.26*a*). Stated differently, the coupled perturbation has a vanishingly small growth time $C'_{\mathrm{c}}=-(\alpha+\beta)\approx0$ in the BNT framework, meaning that the corresponding mode does not grow significantly over the short time scale ϵ^2T_{f}; symmetrically, the undulatory mode is missed in the Trouton analysis as its growth is

https://doi.org/10.1017/jfm.2011.256 Published online by Cambridge University Press

limited by weak bending stress only: this undulatory mode grows much faster than the Trouton model can see – when it is actually unstable.

The hybrid model reveals that the two possible unstable modes are actually in competition in a given physical system, even though they were first revealed using two different mathematical models.

If the system is stable with respect to the undulatory mode, the sheet remains flat over the long time scale T_f. Then, Trouton analysis of buckling applies, and can be used to tell whether a coupled mode develops at long times. Conversely, if the system is unstable with respect to the undulatory mode, the latter grows very rapidly. In this case, the undulatory mode enters into the nonlinear regime after a short delay $\sim 1/C_u \sim \epsilon^2 T_f$, according to the nonlinear analysis of § 4.2. This is much too early for any coupled perturbation predicted by the analysis of § 5 to become significant. As a result, the coupled mode may develop with a long delay on top of the undulatory mode, but the analysis presented here is inapplicable as the base state is not planar. We note that the evolution of the two overlapping patterns at long times cannot be fully described in an asymptotic study in any case, as can be seen, for instance, in Smith (1975).

6.2. *Range of validity of the stability analyses*

We now discuss the range of validity of the stability analyses of §§ 4 and 5. For simplicity, we restrict ourselves to the case of vanishing surface tension.

For the coupled mode, the characteristic growth time is T_f, which is also the time scale of the Trouton model. The Jeffreys number takes the form $Je_c = (\rho g L T_f)/\mu$, where the wavelength L is generally set by the size of the system. Our assumptions require $Je_c \gg 1$, which can be achieved, for instance, if the size L of the system is large enough.

For the undulatory (buckling) mode, the characteristic time for growth is $(z^*/L)^2 T_f$, consistent with the choice of the BNT scaling. It grows at a much faster rate than the coupled mode, as the aspect ratio (z^*/L) is small. Using the scaling $[(\rho g T_f)/(z^*\mu)]^{1/2}$ found for the wavelength of the most unstable mode in (4.16), the Jeffreys number reads $Je_u = [(\rho g h T_f)/\mu]^{1/2}$. Our assumptions require $Je_u \ll 1$, which can be achieved if, for instance, the thickness is small enough.

The validity of our analyses for the buckling and coupled instabilities require $Je_c \gg 1$ and $Je_u \ll 1$, respectively. We note that these conditions are not mutually exclusive. Both can be met if $h \ll \mu/\rho g T_f \ll L$. In such circumstances, both instabilities can be observed concurrently, keeping in mind the limitations mentioned at the end of § 6.1.

6.3. *Orders of magnitude*

We compute here some orders of magnitude for the two modes in the cases of compressional tectonics of the earth's crust and plate glass production. In the two applications, the bath is much less viscous than the two sheets. For the earth's crust floating on the upper mantle we use the following values: $h = 10$ km, $L = 1000$ km, $\mu = 10^{23}$ kg m^{-1} s^{-1}, $\alpha = -10^{-14}$ s^{-1}, $\rho_1 = 2800$ kg m^{-3}, $\rho_2 = 3400$ kg m^{-3} and $\gamma_+ = \gamma_- = 0$ N m^{-1}. These values are only indicative: the rheology of geophysical fluids is non-Newtonian, while the geometry and the loading are complex. For a glass sheet floating on molten tin, we use the following parameters: $h = 3$ mm, $\mu = 10^5$ kg m^{-1} s^{-1}, $\alpha = -0.03$ s^{-1}, $\rho_1 = 2500$ kg m^{-3}, $\rho_2 = 6500$ kg m^{-3} and $\gamma_+ + \gamma_- = 1$ N m^{-1}. Note that the viscosity of glass is highly dependent on temperature, which may impact on the orders of magnitude obtained below. This

https://doi.org/10.1017/jfm.2011.256 Published online by Cambridge University Press

yields the following orders of magnitude for the Jeffreys number:

$$Je_c \approx 30, \quad Je_u \approx 5 \cdot 10^{-1} \text{ (earth's crust)}, \tag{6.7}$$

$$Je_c \approx 10^2, \quad Je_u \approx 10^{-1} \text{ (molten glass)}. \tag{6.8}$$

The values of the Jeffreys number are not always asymptotic and the corresponding predictions are only qualitative. For the undulatory (buckling) mode, the typical growth time $\tau = 1/C_c^{max}$ and wavelength $\lambda = 1/k_{max}$ are given by (4.16). In the earth application, this yields a wavelength of about 150 km and a typical time of 100 000 years. Our nonlinear analysis predicts an amplitude of deformation of $\sim h = 10$ km in the same typical time. The length scales are satisfying while the time scale is an order of magnitude too small. This might be ascribed to the various simplifications of the problem. In the glass application, we obtain a wavelength of several centimetres $\lambda \approx 10$ cm and a typical time $\tau \approx 10^{-1}$ s. The nonlinear analysis predicts that the amplitude of deformation reaches the thickness of the glass sheet in this typical time. The wavelength matches the typical wavelengths of imperfections observed on float glass, and correctly predicts the orientation of stripes perpendicular to the direction of stretching (buckling mode). However, we cannot predict the amplitude because the process is intrinsically non-stationary: the flow is compressive and extensional according to the position along the bath.

The coupled mode is more unstable for small wavenumbers. As a result, its wavelength and direction are controlled by the geometry of the system at large scale. We shall only estimate the typical growth time $\tau = 1/C_c^{max}$, where C_c^{max} from (5.18). In the earth application the typical growth time is 6 million years, which is a sensible geological time scale. This mode might correspond to the variable thickness of the crust across mountain ranges. In the glass application, the typical growth time is 10^2 s, which is comparable to the typical residence time of the glass in the float process, which could explain the large-scale imperfections of the thickness of float glass.

6.4. *Conclusion*

We have derived a reduced, two-dimensional model for thin viscous sheets subjected to arbitrary forces applied in the bulk or on the interfaces. The equations are compact, and expressed in terms of thickness-averaged quantities such as position, velocity, in-plane stress and bending moments. Such formulations have been extensively used for elastic plates and shells, but have received much less attention in the context of viscous sheets. Our equations are valid for weak deflections from a straight configuration, and are well suited to the analysis of buckling. The models based on the Trouton and BNT scalings were derived in a unified manner. We presented a comprehensive analysis of the buckling of thin floating sheets for arbitrary base flows. A planar base flow can become unstable when it induces a large enough contraction along some tangent direction. We identified a buckling mode with a wavenumber aligned with the direction of most vigorous contraction, and a coupled mode with a wavenumber perpendicular to it. In addition, the nonlinear evolution of buckling was studied, revealing a cross-over between the short-time, exponential evolution of the amplitude, as predicted by linear stability, to a large-time, square-root evolution of the amplitude, as imposed by kinematics. The equations for thin viscous sheets subjected to external forces derived in this paper provide a framework applicable to a variety of problems and geometries, and can serve as a basis for an efficient numerical implementation.

https://doi.org/10.1017/jfm.2011.256 Published online by Cambridge University Press

We would like to thank P. Clavin and J.-M. Chomaz for suggesting useful bibliographical references. Careful reviews by N. Ribe and two anonymous referees were extremely useful for the improvement of the initial manuscript.

Appendix A. Identities for slice-based operators

Taking the derivative with respect to x of the definition (2.3*a*) for the thickness-integral operator I, we have for a fixed time

$$[I\cdot(\phi_{,x})](x)=\frac{\mathrm{d}[I\cdot\phi]}{\mathrm{d}x}-\phi(x,z_+(x))\frac{\mathrm{d}z_+}{\mathrm{d}x}+\phi(x,z_-(x))\frac{\mathrm{d}z_-}{\mathrm{d}x}. \tag{A 1}$$

The two last terms come from the fact that the interval of integration, $z_-(x)\leqslant z\leqslant z_+(x)$, has non-constant endpoints. We refer to this formula as 'integration by parts along the z direction'.

When the argument of the operator I is an exact derivative with respect to z, we can carry out the integration explicitly:

$$[I\cdot(\phi_{,z})](x)=\phi(x,z_+(x))-\phi(x,z_-(x)). \tag{A 2}$$

These identities can be turned into identities for the first-moment operator J by a special choice of the function ϕ:

$$\phi(x,z)=(z-H(x))\gamma(x,z) \tag{A 3}$$

for some function $\gamma(x,z)$. For that particular choice of ϕ, the definition (2.3*b*) of J reads:

$$[I\cdot\phi](x)=[J\cdot\gamma](x). \tag{A 4}$$

Substituting into the first identity (A 1), we have

$$\begin{aligned}&[I\cdot(-H_{,x}\gamma)](x)+[J\cdot(\gamma_{,x})](x)\\&\quad=\frac{\mathrm{d}[J\cdot\gamma]}{\mathrm{d}x}-\frac{h(x)}{2}(z_{+,x}(x)\gamma_+(x)+z_{-,x}(x)\gamma_-(x)),\end{aligned} \tag{A 5}$$

where $\gamma_\pm(x)$ is a shorthand notation for $\gamma(x,z_\pm(x))$.

Substituting into the second identity (A 2), we find

$$[I\cdot\gamma](x)+[J\cdot(\gamma_{,z})]=\frac{h(x)}{2}(\gamma_+(x)+\gamma_-(x)). \tag{A 6}$$

Another identity follows from the definitions (2.3*d*) and (2.3*e*) of the operators A and χ:

$$[\chi\cdot\phi](x)=\tfrac{1}{2}([A\cdot\phi](x,z_+(x))+[A\cdot\phi](x,z_-(x))). \tag{A 7}$$

A last set of identities allows one to rewrite the composition of the operator A with either I or J in terms of the first and second moments J or K:

$$[I\cdot[A\cdot\phi]](x)=h(x)[\chi\cdot\phi](x)-[J\cdot\phi](x), \tag{A 8a}$$

$$[J\cdot[A\cdot\phi]](x)=\frac{h^2(x)}{8}[I\cdot\phi](x)-[K\cdot\phi](x). \tag{A 8b}$$

These identities follow from a permutation of the two integrals associated with the operators on the left-hand sides. The most direct proof is to notice that both sides of each equality are linear forms of ϕ, and to check the equalities when ϕ is a Dirac function, $\phi(z)=\delta_D(z-z_0)$, studying the cases $z_-<z_0<H$ and $H<z_0<z_+$ separately. Details of the proof are left to the reader.

https://doi.org/10.1017/jfm.2011.256 Published online by Cambridge University Press

Appendix B. Interpretation of the equations of equilibrium

Here, we propose an interpretation of the (2.14) and (2.20) for the equilibrium of a thin two-dimensional sheet, by showing equivalence with the Kirchhoff equations for a thin rod. The equations of equilibrium (2.45) and (2.46*b*) in a three-dimensional geometry have a similar structure, and can be interpreted similarly.

In a thin elastic rod, the resultant and moment of internal stress $\boldsymbol{S}$ over a cross-section are denoted by $\boldsymbol{n}(x)$ and $\boldsymbol{m}(x)$, and the balance of force and moment over a small length of the rod is expressed by the classical Kirchhoff equations:

$$\boldsymbol{n}'(x) + \boldsymbol{p}(x) = \boldsymbol{0}, \tag{B 1}$$

$$\boldsymbol{m}'(x) + \boldsymbol{t}(x) \times \boldsymbol{n}(x) + \boldsymbol{q}(x) = \boldsymbol{0}. \tag{B 2}$$

With the right-hand sides set to zero, this defines the equations of equilibrium. Here, $\boldsymbol{p}(x)$ and $\boldsymbol{q}(x)$ are the lineic densities of applied forces and moments, and $\boldsymbol{t}(x)$ is the tangent to the centreline.

We are concerned with a two-dimensional geometry, restricted to the (x, z) plane: $\boldsymbol{n} = (n_x, 0, n_z)$, $\boldsymbol{m} = (0, m_y, 0)$, $\boldsymbol{p} = (p_x, 0, p_z)$, $\boldsymbol{q} = (0, q_y, 0)$. In addition, we consider the small-slope approximation, $\boldsymbol{t} = (1, 0, H_{,x})$, the quantity $H_{,x}$ being small, of order ϵ. Projection of Kirchhoff equations onto the axes yields

$$n_{x,x} + p_x = 0, \tag{B 3}$$

$$n_{z,x} + p_z = 0, \tag{B 4}$$

$$m_{y,x} - n_z + H_{,x} n_x + q_y = 0. \tag{B 5}$$

Elimination of the normal internal force n_z by (B 5) and substitution into (B 4) yield

$$m_{y,xx} + (H_{,x} n_x)_{,x} + q_{y,x} + p_z = 0. \tag{B 6}$$

We can identify the axial balances of forces (2.14) and (B 3) on one hand, and the transverse balances of forces (2.20) and (B 6) on the other hand, with the following variables:

$$n_x = N_{xx}, \tag{B 7}$$

$$m_y = M_{xx}, \tag{B 8}$$

$$p_x = [I \cdot f_x^{(0)}], \tag{B 9}$$

$$p_z = [I \cdot f_z^{(1)}], \tag{B 10}$$

$$q_y = [J \cdot f_x^{(0)}]. \tag{B 11}$$

REFERENCES

BARNES, G. & WOODCOCK, R. 1958 Liquid rope-coil effect. *Am. J. Phys.* **26**, 205–209.

BENJAMIN, T. B. & MULLIN, T. 1988 Buckling instabilities in layers of viscous liquid subjected to shearing. *J. Fluid Mech.* **195**, 523–540.

BIOT, M. A. 1964 Theory of viscous buckling of multilayered fluids undergoing finite strain. *Phys. Fluids* **7**, 855–861.

BLAKE, K. R. & BEJAN, A. 1984 Experiments on the buckling of thin fluid layers undergoing end-compression. *Trans. ASME: J. Fluids Engng* **106**, 74–78.

BOUDAOUD, A. & CHAÏEB, S. 2001 Singular thin viscous sheet. *Phys. Rev.* E **64**, 050601.

BUCKMASTER, J. D. & NACHMAN, A. 1978 The buckling and stretching of a viscida. Part II. Effects of surface tension. *Q. J. Mech. Appl. Math.* **31**, 157–168.

BUCKMASTER, J. D., NACHMAN, A. & TING, L. 1975 The buckling and stretching of a viscida. *J. Fluid Mech.* **69**, 1–20.

https://doi.org/10.1017/jfm.2011.256 Published online by Cambridge University Press

CHARRU, F. 2007 *Instabilités Hydrodynamiques*, CNRS edn. EDP Sciences.

CIARLET, P. G. 1980 A justification of the von Kármán equations. *Arch. Rat. Mech. Anal.* **73** (4), 349–389.

CRUICKSHANK, J. O. & MUNSON, B. R. 1982 A theoretical prediction of the fluid buckling frequency. *Phys. Fluids* **25**, 1935–1937.

DA SILVEIRA, R., CHAÏEB, S. & MAHADEVAN, L. 2000 Rippling instability of a collapsing bubble. *Science* **287** (5457), 1468–1471.

DEBRÉGEAS, G., DE GENNES, P. G. & BROCHARD-WYART, F. 1998 The life and death of 'bare' viscous bubbles. *Science* **279** (5357), 1704–1707.

DRET, H. L. & RAOULT, A. 1995 The nonlinear membrane model as variational limit of three-dimensional nonlinear elasticity. *J. Math. Pures Appl.* **75**, 551–580.

DYSON, R. J. & JENSEN, O. E. 2010 A fibre-reinforced fluid model of anisotropic plant cell growth. *J. Fluid Mech.* **655**, 472–503.

ENGLAND, P. & MCKENZIE, D. 1983 Correction to: A thin viscous sheet model for continental deformation. *Geophys. J. R. Astron. Soc.* **73**, 523–532.

FILIPPOV, A. & ZHENG, Z. 2010 Dynamics and shape instability of thin viscous sheets. *Phys. Fluids* **22**, 023601.

GRIFFITHS, I. M. & HOWELL, P. D. 2007 The surface-tension-driven evolution of a two-dimensional annular viscous tube. *J. Fluid Mech.* **593**, 181–208.

GRIFFITHS, I. M. & HOWELL, P. D. 2008 Mathematical modelling of non-axisymmetric capillary tube drawing. *J. Fluid Mech.* **605**, 181–206.

GRIFFITHS, I. M. & HOWELL, P. D. 2009 The surface-tension-driven retraction of a viscida. *SIAM J. Appl. Math.* **70** (5), 1453–1487.

GUILLOU-FROTTIER, L., BUTTLES, J. & OLSON, P. 1995 Laboratory experiments on the structure of subducted lithosphere. *Earth Planet. Sci. Lett.* **133**, 19–34.

HOWELL, P. D. 1996 Models for thin viscous sheets. *Eur. J. Appl. Math.* **7**, 321–343.

JEFFREYS, H. 1925 The flow of water in an included channel of rectangular section. *Phil. Mag.* **49**, 793.

JOHNSON, A. M. & FLETCHER, R. C. 1994 *Folding of Viscous Layers: Mechanical Analysis and Interpretation of Structures in Deformed Rock*. Columbia University Press.

KÜCKEN, M. & NEWELL, A. C. 2004 A model for fingerprint formation. *Europhys. Lett.* **68**, 141–146.

LIFSCHITZ, A. & HAMEIRI, E. 1991 Local stability conditions in fluid dynamics. *Phys. Fluids* A **3** (11), 2644.

MAHADEVAN, L., RYU, S. & SAMUEL, A. D. T. 1998 Fluid rope trick investigated. *Nature* **392**, 140.

MANNEVILLE, P. 2004 *Instabilities, Chaos and Turbulence*. Imperial College Press.

MARHEINEKE, N. & WEGENER, R. 2009 Asymptotic model for the dynamics of curved viscous fibres with surface tension. *J. Fluid Mech.* **622**, 345–369.

O'KEEFE, J. A. 1969 Water on the moon and a new nondimensional number. *Science* **163**, 669.

PEARSON, J. R. A. 1985 *Mechanics of Polymer Processing*. Elsevier.

PEARSON, J. R. A. & PETRIE, C. J. S. 1970*a* The flow of a tubular film. Part 1. Formal mathematical representation. *J. Fluid Mech.* **40** (1), 1–19.

PEARSON, J. R. A. & PETRIE, C. J. S. 1970*b* The flow of a tubular film. Part 2. Interpretation of the model and discussion of solutions. *J. Fluid Mech.* **42** (3), 609–625.

PERAZZO, C. A. & GRATTON, J. 2010 Convergent flow in a two-layer system and mountain building. *Phys. Fluids* **22**, 056603.

PFINGSTAG, G., AUDOLY, B. & BOUDAOUD, A. 2011 Thin viscous sheets with inhomogeneous viscosity. *Phys. Fluids* (submitted).

PILKINGTON, A. 1969 The float glass process. *Proc. R. Soc. Lond.* A **314**, 1–25.

RAMBERG, H. 1981 *Gravity, Deformation and the Earth's Crust*, 2nd edn. Academic.

RAYLEIGH, J. W. 1896 *The Theory of Sound*. Macmillan.

RIBE, N. M. 2001 Bending and stretching of thin viscous sheets. *J. Fluid Mech.* **433**, 135–160.

https://doi.org/10.1017/jfm.2011.256 Published online by Cambridge University Press

RIBE, N. M. 2002 A general theory for the dynamics of thin viscous sheets. *J. Fluid Mech.* **457**, 255–283.

RIBE, N. M., STUTZMANN, E., REN, Y. & VAN DER HILST, R. 2007 Buckling instabilities of subducted lithosphere beneath the transition zone. *Earth Planet. Sci. Lett.* **254**, 173–179.

SCHEID, B., QUILIGOTTI, S., TRAN, B. & STONE, H. A. 2009 Lateral shaping and stability of a stretching viscous sheet. *Eur. Phys. J.* B **68** (4), 487–494.

SMITH, R. B. 1975 Unified theory of the onset of folding, boudinage, and mullion structure. *Bull. Geol. Soc. Am.* **86**, 1601–1609.

STEELE, C. R. 2000 Shell stability related to pattern formation in plants. *Trans. ASME: J. Appl. Mech.* **67** (2), 237.

STOKES, G. G. 1845 On the theories of the internal friction of fluids in motion and of the equilibrium and motion of elastic solids. *Trans. Camb. Phil. Soc.* **8**, 287.

SULEIMAN, S. M. & MUNSON, B. R. 1981 Viscous buckling of thin fluid layers. *Phys. Fluids* **24**, 1–5.

TAYLOR, G. I. 1968 Instabilities of jets, threads and sheets of viscous fluid. In *Proceedings of the 12th International Congress of Applied Mechanics*, pp. 382–388. Springer.

TORO, R. & BURNOD, Y. 2005 A morphogenetic model for the development of cortical convolutions. *Cereb. Cortex* **15**, 1900–1913.

VAN DE FLIERT, B. W., HOWELL, P. D. & OCKENDON, J. R. 1995 Pressure-driven flow of a thin viscous sheet. *J. Fluid Mech.* **292**, 359–376.

YARIN, A. L., GOSPODINOV, P. & ROUSSINOV, V. I. 1994 Stability loss and sensitivity in hollow fibre drawing. *Phys. Fluids* **6** (4).

ZEL'DOVICH, Y. B., ISTRATOV, A. G., KIDIN, N. I. & LIBROVICH, V. B. 1980 Flame propagation in tubes: hydrodynamics and stability. *Combust. Sci. Technol.* **24** (1–2), 1–13.

https://doi.org/10.1017/jfm.2011.256 Published online by Cambridge University Press